A NEW DRAG MEASUREMENT SYSTEM FOR WIND TUNNEL TESTING OF THE RACING BICYCLE AND RIDER TO DETERMINE A LOW DRAG CONFIGURATION

THESIS

Brian A. Parker, Captain, USAF
AFIT/GAE/ENY/94D-17

DEPARTMENT OF THE AIR FORCE
AIR UNIVERSITY
AIR FORCE INSTITUTE OF TECHNOLOGY

Wright-Patterson Air Force Base, Ohio

AFIT/GAE/ENY/94D-17

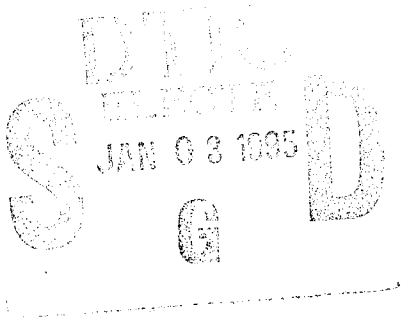

A NEW DRAG MEASUREMENT SYSTEM FOR WIND TUNNEL TESTING OF THE RACING BICYCLE AND RIDER TO DETERMINE A LOW DRAG CONFIGURATION

THESIS

Brian A. Parker, Captain, USAF
AFIT/GAE/ENY/94D-17

Approved for public release; distribution unlimited

AFIT/GAE/ENY/94D-17

A NEW DRAG MEASUREMENT SYSTEM FOR WIND TUNNEL TESTING OF THE RACING BICYCLE AND RIDER TO DETERMINE A LOW DRAG CONFIGURATION

THESIS

Presented to the Faculty of the School of Engineering
of the Air Force Institute of Technology Air University
In Partial Fulfillment of the
Requirements of the Degree of
Master of Science in Aeronautical Engineering

Brian A. Parker
Captain, USAF

December 1994

Approved for public release; distribution unlimited

ACKNOWLEDGEMENTS

Projects of any magnitude are rarely the sole product of any one person. This thesis relied on the expertise and support of many individuals that I would like to acknowledge.

The topic for thesis would not have been possible without the sponsorship of Mr. Bruce Campbell, WL/XPT. Likewise, I am indebted to my advisor, Dr. Milton Franke, for supporting a somewhat nontraditional topic, showing genuine interest in the project and giving me the leeway to make mistakes and learn from them. I am a better Air Force officer for having endured the process.

The successful completion of this project weighed heavily on the parts and equipment fabricated by the AFIT model shops. At project completion, every person from the shop had made a part (or repaired the ones I broke) for this new system. Specifically, I would like to thank the shop supervisor, Mr. Jack Tiffany, Mr. Dave Driscoll, Mr. Jan LeValley, Mr. Tim Hancock, and Mr. Ron Ruley.

Considerable effort was also expended by our tunnel operator and technician, Mr. Charles McNeeley. His operational and electronics experience was invaluable to this effort.

I would like to thank my research partner, Capt Alan Elledge, for not only developing the new wind tunnel data acquisition software but also for his teamwork on the tunnel characterization, cylinder test case data and troubleshooting all the numerous problems we encountered.

Finally, my greatest thanks go to my wife for her help, encouragement and prodding that kept me going even though it seemed as though I would never finish.

TABLE OF CONTENTS

LIST OF FIGURES

Page

LIST OF TABLES

LIST OF SYMBOLS

AFIT	Air Force Institute of Technology
A	area
b	calibration curve intercept
c	sensitivity of Wheatstone bridge/strain gage system
C	calibration matrix
C_D	drag coefficient
D	drag force
e_i	Wheatstone bridge input excitation
e_o	Wheatstone bridge output voltage
E	modulus of elasticity
f	applied force
h	thickness of flexure beam
l	length of force moment arm
m	calibration curve slope
p	static pressure
q	dynamic pressure
r	force range of flexure
s	total leg spacing from frame
sb	solid blockage correction factor
S_f	fatigue strength of material
s_g	strain gage gain factor
USCF	United States Cycling Federation
v	measured voltage
V	volume

w	weight
wb	wake blockage correction factor
x	length of flexure beam
y	width of flexure beam

Greek Symbols

ε	strain

Subscripts

avg	averaged quantity
norm	normalized quantity

ABSTRACT

This study investigated the application of splitter plate effects to reduce the aerodynamic drag of the racing bicycle and rider system. A sensitive, low-force, beam-type, single-component balance was developed to provide drag measurements accurate to within 0.053 N (0.012 lb_f). The performance of the new system was verified by comparing the measured drag on a three-dimensional, right-circular cylinder model, 0.127 m (5.0 in) in diameter and 0.610 m (24 in) long, with the results from a commercial balance and other similar data. The bicycle and rider model consisted of a full-scale mannequin comprising only the hips, legs and feet, mounted on a regulation 0.48 m (19 in) size bicycle. Rotation of the wheels and a stationary ground plane were also simulated. Two frame configurations in conjunction with a disk type wheel were tested to determined the lowest drag configuration for narrow and wide spacing of the rider's legs. The results show that for the standard tube construction frame, the conventional wisdom to streamline as much as possible prevails. When an aerodynamic frame was tested, the overall drag was reduced. Although the standard spacing still provided the lowest drag configuration, any further streamlining showed an increase in drag.

I. INTRODUCTION

Almost any vehicle traveling through air can benefit from improved aerodynamics. When taken to an extreme, such as in competitive bicycle racing, the advantage from better aerodynamics could mean the difference between winning or losing. The primary resistance forces on a cyclist are aerodynamic drag and rolling friction. At speeds over 40 km/h (25 mph), drag is 90% of the total resistive force on a cyclist [1]. Typical total drag values for a bicycle and rider vary between 26.7-35.6 N (6-8 lb_f) depending on the equipment used. Analysis of the bike and rider system reveals that of that 90% the rider is responsible for roughly two-thirds of the total aerodynamic drag and the bike the remaining one-third [2]. The drag consists of pressure and skin friction drag. Of these two, pressure drag is the dominant component that results from unbalanced pressures on the object due to air flow separation over the surface of the object [2]. Streamlining the object or modifying the wake to recover the pressure will reduce the drag.

Since the sustained output power of humans is typically only 400 W (0.54 hp), even very small differences in drag will substantially improve the performance of an elite cyclist racing at speeds between 40-56 km/h (25-35 mph). As shown in Table 1, reducing the drag by only 0.10 N (0.02 lb_f or roughly the weight of three American pennies) will gain a quarter second at the finish line for a 4000 meter race [3].

Table 1. The Effect of Aerodynamic Drag Reduction on Race Times [3]

Drag Decrease N (lb_f)	Distance Advantage m/km (ft/mile)	Time Decrease for a 1000m Time Trial (sec)	Time Decrease for a 4000m Pursuit Race (sec)
0.10 (0.02)	0.95 (5.0)	0.07	0.28
0.20 (0.04)	1.89 (10.0)	0.12	0.62
0.40 (0.09)	3.79 (20.0)	0.23	1.12
0.78 (0.18)	7.77 (41.0)	0.47	2.22
1.18 (0.27)	11.55 (61.0)	0.7	3.39
1.57 (0.35)	17.23 (91.0)	0.94	4.53
1.96 (0.44)	21.02 (111.0)	1.17	5.62

Viewed another way, this drag reduction would allow a 0.95 m/km (5 ft per mile) distance advantage such that at the end the race (which typically ends in a photo finish) one would have a 3.81 m (12.5 ft) lead or nearly 2.5 bike lengths. Thus, the search for even these small reductions in drag is worthwhile.

Historically, Union Cycliste Internationale (UCI), the governing body of international cycling, impeded any aerodynamic improvement in bicycle racing by enforcing strict rules and regulations. Consequently, most technological changes in equipment were limited to component quality and materials rather than frame designs. Recent rule revisions, however, have allowed rapid development and advances in the aerodynamic configuration of the bicycle frame itself. Indeed, recent frame designs for track and time trial use appear more as an airfoil than a bicycle [4].

Most manufacturers have placed emphasis on the aerodynamics of components (wheels, frames and helmets) [5]. In addition, racing teams and Olympic committees focused their work on rider positioning because of the rider's greater influence on drag. However, studies that concentrated on the bike itself showed it to be a likely candidate for aerodynamic improvement as well [6]. The findings of the more recent aerodynamic research in this area were not unexpected -- the more streamlined the object the lower the drag [7]. Indeed, some of these new aerodynamic frame configurations were able to reduce the drag by almost half -- a savings that would provide an advantage to any racer. Unfortunately, when these frames were integrated with the rider the drag reduction was not as optimal as the individual systems. The integrated bicycle and rider system in this case realized only a 14% improvement. Further research is needed to determine why the bicycle and rider system did not show the total benefits of the aerodynamic components and what can be changed to reduce the drag of the systems as a whole.

The ability to measure these small values of drag is critical to this study. However, most commercial wind tunnel force balances do not have nor do they need this level of resolution. For instance, the Huffy Corporation of Dayton, Ohio previously attempted similar tests with aerodynamically designed bikes in the AFIT 1.5-m (5-ft) wind tunnel. Unfortunately, they were unable to draw conclusions from the data because the accuracy of the measurements from the existing balance exceeded the very changes in drag they were attempting to show [8].

This investigation had two objectives. The first objective established a new low speed, low force capability for the AFIT 1.5-m (5-ft) wind tunnel. The low speed characteristics of the tunnel were determined through a static and dynamic pressure survey. The low force capability was developed in two parts. One part consisted of the

design, fabrication and testing of a special single component (drag) balance. The second part of the low force system consisted of a new data acquisition system to support the new balance. The details of the data acquisition system are included in Capt Elledge's thesis [13]. Confidence and verification of both parts of the new force system were established through drag measurements of a three-dimensional cylinder model with a known C_D. The final objective was to determine the lowest drag configuration of an integrated racing bicycle and rider model by varying the spacing between the rider's legs and the bicycle frame. The hypothesis that a minimum spacing exists is based on splitter plate theory.

II. THEORY

Splitter Plate Theory

By idealizing the bicycle frame and rear wheel as a flat plate and the rider's legs as cylinders, then the geometry is similar to a splitter plate and cylinder arrangement. When viewed this way, the bike and rider configuration would appear to lend itself to aerodynamic improvement through the application of splitter plate theory.

A splitter plate is a passive, simple, and effective system that works by forming a physical boundary between the vortices in the wake behind a bluff body [9]. Since the vortices are unable to coalesce downstream, there is less turbulence in the wake and therefore less drag on the body. The plates themselves are simply thin flat plates either attached to, located downstream of, or sometimes side by side of the bluff body, i.e., cylinder, sphere, blunt airfoil, etc.

Cylinder and splitter plate research [10], in ideal two-dimensional conditions, indicate that the splitter plate should be located anywhere from 0 to 5 diameters (of the cylinder) downstream of the bluff body and have a gap between the plate and cylinder of 0.2 times the diameter. Without any gap, the plate and cylinder form one large bluff body with a large separated region behind this arrangement. Allowing some flow through the gap reduces the separated region. The theory suggests that there exists a minimum spacing between the bicycle frame and disk wheel (flat plate) and the rider's legs (cylinders) resulting in an optimal low drag configuration. This spacing factor will be determined for the more complex interaction flow of the bicycle and rider. (The spacing

will be based on the distance between the rider's feet relative to the bicycle frame and is illustrated in more detail in Section III.)

Hence, the optimal spacing configuration should allow the air to flow cleanly over the frame with the bonus of the wake shed from the rider's legs reattaching to the rear wheel downstream. Thus the overall wake should be reduced. If the spacing is too wide, the vortices shed from the legs will form downstream of the wheel (splitter plate) and the drag will increase. Also, significant drag should result if the leg spacing is too narrow because the bicycle and legs form one large bluff body with a profound wake.

III. TEST EQUIPMENT

Low Force Measurement System

The wind tunnel's existing aerodynamic load measurement system was not adequate for this project. The balance had to carry a large moment as the bicycle weight (approximately 10 kg (22 lb_f)) would be cantilevered off the end. Secondly, the 0.0127 m (0.5 in) diameter commercial six-component balance was designed for a maximum axial force of 222.4 N (50 lb_f) which, if the balance was accurate to 1% of full scale or 2.22 N (0.5 lb_f), would not meet the resolution requirements of this project.

Therefore, a new low force measurement capability was needed to meet the 0.04 N (0.01 lb_f) drag resolution requirement of this project. Compared to the traditional horizontal sting arrangement, the new system alleviated the moment from the model weight by mounting the sting to the ceiling of the tunnel, carrying the model vertically. As a result of this vertical arrangement, the drag on the model could be, unlike other balances, measured directly by the moment generated from the drag on the model. Directly measuring the load avoided any frictional losses or other errors from connecting hardware linkages and bearings.

To measure the direct moment, a flexure or balance was placed between the model and the sting as shown in Figure 1. The moment arm from the model to the flexure also helped increase the resulting moment of a small force. Since the objective of this study was focused primarily on the measurement of changes in drag relative to a baseline configuration, only a single component (drag) flexure was configured.

With this vertical and single component balance arrangement, certain characteristics of the system must be recognized when reviewing the resulting drag measurements. Static axial loads and moments from the weight of the model are removed from the output by taking a "no wind" data point then subsequently subtracting this value from the final measurement. This effectively references the data to a known condition. The data reduction details are found in Section V. When the air is flowing over the model, the possibility of unwanted moments also exists. For example, a small amount of unbalanced lift on the front wheel would cause the flexure to register additional moment. The existence of unbalanced lift is unlikely because the bicycle is mounted more like a "weathervane", yawing rather than pitching. In addition, the bicycle results for the single component balance compared favorably with other historical results indicating the balance was performing correctly.

The size of the flexure beam was based on several parameters. The small changes in drag that were expected from the configuration changes required a highly sensitive instrument. In addition, the full-scale range of the device should be limited to the maximum expected drag to improve accuracy. Specifications of the strain gages and operational performance also had an impact on the final sizing of the flexure. Based on linear beam theory [11], the flexure was sized to give the greatest sensitivity according to

$$c = \frac{6 s_g l e_i}{E b h^2} \tag{1}$$

where s_g is the strain gage gain factor, l is the length of the force moment arm to the center of the strain gage, e_i is the excitation voltage applied to the Wheatstone bridge and strain gage system, E is the modulus of the material, and b and h are the width and

thickness of the beam respectively. The sensitivity, c, is equivalent to the slope of the curve that results from the calibration of the flexure. As one can see, the greatest sensitivity results from an increasingly long, thin beam. However, the resulting beam would have to satisfy a constraint (recommended by the strain gage manufacturer) that the beam provide at most 1500 μstrain at full scale according to

$$\varepsilon = \frac{6fl}{Ebh^2} \tag{2}$$

where f is the maximum expected force. Furthermore, the beam's maximum range calculated from,

$$r = \frac{S_f bh^2}{6l} \tag{3}$$

with S_f equal to the fatigue strength of the material, was limited to the maximum expected drag.

Based on the above equations, an optimization routine was employed to determine the values for l, b and h. The optimization for the cylinder testing parameters produced a flexure that performed well operationally and resulted in a sensitivity close to predicted. However, when the beam, sized for the bicycle testing, was utilized in the tunnel it demonstrated an unacceptable level of torsional flexibility. As a result, the beam thickness, h, was increased. To compensate for the reduction in sensitivity (sensitivity and strain vary inversely with the square of h), the excitation voltage applied to the bridge was increased from a nominal 6 v to 10 v.

Several iterations of the flexure's material, strain gages and adhesives were also required before an acceptable combination was found. Stainless steel (because of its thermal properties) was initially chosen as the flexure material when highly sensitive semiconductor strain gages were a possible measurement device. The stainless steel exhibited severe hysterisis however when the foil type gages were used. It is not recommend that stainless steel be used in the future for this reason. The final configuration was made from 2024-T8 aluminum with the characteristics as listed in Table 2 for the cylinder and bicycle testing. The two versions were required based on the expected drag of each model.

Table 2. Flexure Properties for Cylinder and Bicycle Drag Measurements

Flexure	$Drag_{pred}$ N (lb_f)	x m (in)	b m (in)	h m (in)	c_{pred} V/N (V/lb_f)	r_{pred} N (lb_f)
Cylinder	17.8 (4.0)	0.050 (2.00)	0.010 (0.40)	0.006 (0.25)	1.18e-3 (5.26e-3)	19.62 (4.41)
Bicycle	35.6 (8.0)	0.050 (2.00)	0.001 (0.35)	0.001 (0.35)	1.01e-3 (4.48e-3)	39.72 (8.93)

To measure the strain induced in the beam, foil type strain gages were used. Transducer class strain gages, model N2A-13-T006N-350 from Micro Measurements Group, Inc., were used. These gages are a foil type with a nominal gage factor of 2.1 and a resistance of 350Ω. On several of the iterations, MBOND 200 (essentially super glue) adhesive was used. Although easy to use, this adhesive proved to be too brittle when fully cured and would eventually fail under the dynamics of the wind tunnel. The solution was

MBOND 600 adhesive which is heat and pressure cured. The resulting bond is longer lasting and allows the strain gage to more accurately reproduce the actual strain in the beam. The gages were wired into a full Wheatstone bridge that provided increased sensitivity and thermal compensation. The 350Ω resistance of the gage allowed then application of a 10 volt excitation voltage to the bridge to required to obtain the desired sensitivity.

Data Acquisition System

The configuration of the new drag measurement system necessitated major changes in the data acquisition system previously in use at the AFIT 1.5m (5-ft) wind tunnel. The prior system consisted of a Hewlett-Packard HP3852A Data Acquisition/Control Unit (DACU) managed by the WIND software [12]. The software modifications to adapt the WIND software calibration and data processing subroutines from the six-component balance to the single component balance were considered too cumbersome because the software was in an outdated version of the Pascal computer language. In addition, the DACU firmware would not allow the system to be configured to output time histories. Time histories were considered an important analysis and trouble shooting tool. As a result of the above, a new data acquisition system was pursued.

The new digital data acquisition system consisted of three major components -- an AT-MIO-16L software configurable data acquisition board from National Instruments Corp.®, Lab VIEW™ software, and a 486 PC. Lab VIEW ™ software is a graphical programming language for development of data acquisition and analysis applications. It is capable of providing complete control of the data acquisition board for sampling rate, number of samples, gain, and input range. In addition, data processing such as averaging,

filtering and FFTs are possible. Using this software, an application specific to the wind tunnel and this testing was created by Capt Alan Elledge as part of his thesis [13].

The data acquisition board provided 12 bit digital to analog conversion (ADC) for up to 16 analog inputs in the single ended mode or 8 inputs in the double ended mode. The double ended configuration resulted in the lowest noise levels and was used for this testing. The 12 bit ADC provided accuracy's and ranges according to Table 3.

Table 3. Voltmeter Range and Associated Precision

Input Range (Volts)	Resolution (Volts)
-10.0 to + 10.0	4.88 e-3
-1.0 to + 1.0	488 e-6
-0.10 to + 0.10	48.8 e-6
-0.020 to + 0.020	9.76 e-6

The board was software configurable and allowed the voltage range for each channel to be set independently. The range of the one component balance was such that it was set to the $\pm$ 0.10 range. The other measurement channels were set to the appropriate range and accuracy based on their respective full scale values.

Before the completion of the new acquisition system, the static pressure data used to evaluate tunnel performance was collected using the WIND software, and the Pressure Systems Inc. 780B Pressure Measurement System and Pressure Calibrate Unit. A 1 psid electronically scanned pressure (ESP) module was used to collect data from 22 static ports

located at the tunnel station shown in Figure 2. The system self calibrates before each data collection session resulting in an estimated accuracy of 0.1% of full scale.

Cylinder Model

The three-dimensional right-circular cylinder model used to compare the drag from the single component balance with the six-component commercial balance was 0.127 m (5 in) in diameter and 0.61 m (24 in) long. The resulting height to span ratio of 0.21 corresponds to a C_D of 0.75 at a Reynolds number of 10^5 according to Hoerner [14]. The model was constructed from acrylic Plexiglas with a machined insert for mounting to the balances. Figures 3a and 3b show upstream and downstream views of the model as installed in the wind tunnel using the six-component balance. The installation for the single component balance is shown in Figures 3c and 3d.

Bicycle Model

For this study, a track type bicycle was simulated. It is this form of racing that would benefit the most from aerodynamic improvements because typically there is not a large pack in which to draft in. An actual competition track bicycle was not available so a standard full size 0.49 m (19.25 in) road bike was modified by removing the brake hoods, cabling, derailleurs, and extra chain ring. The bicycle was nearly complete except for the chain which was removed for operational reasons. The bottom bracket, where the crank arms of the pedals attach through bearings to the frame, was 0.70 m (2.76 in) wide. The spacing variations were relative to this fixed distance as sketched in Figure 4. Tests were performed with the main triangle of the frame open, as is usually the case, and also enclosed in a mylar skin to simulate an aerodynamic bike frame. This concept is idealized in the sketch of Figure 5.

The USCF provided aerodynamic wheels for this testing. A 0.61 m (24 in) skirted wheel was used in front and a 0.61 m (24 in) disk type wheel in the rear. The disk wheel, shown in Figure 6, was a "sew-up" type wheel with a racing slick tire. The profile of the disk was completely flat and not lenticular as some are. Rotation of the wheel was created by a high speed pneumatic air tool mounted in a streamlined position on the frame and in contact with the bicycle wheel through a rubber wheel. Wheel rpm was monitored by an optical sensor and a Racal-Danna 1992 Nanosecond Universal Counter collocated with the drive mechanism.

The entire model was placed over a 1.8 m (6 ft) long, 0.6 m (2 ft) wide ground plane secured to the tunnel floor. The wheels were within in (0.25 in) of the ground plane. This was compromise due to the setup since in reality the wheel is in contact with the road and no flow under the wheel is possible. The effects of the ground plane and bicycle interaction were not investigated.

Mannequin

The lower half of a mannequin was used to simulate the rider's legs. Only the legs were simulated because of the complexity, blockage and interference a full mannequin presented. Dr. Chester Kyle, technical director for related aerodynamic testing for the USCF, indicated that in his experience the torso should have little effect on the area of the bicycle this testing was concerned with [15]. As it was, the frontal area of the half mannequin and bicycle was 0.29 m^2 (3.13 ft^2) representing 17% of the tunnel cross sectional area. Traditionally the model should not take more than 20% to avoid causing large variations in tunnel dynamic pressure. As a result, corrections for blockage effects were necessary and are described in greater detail in Section V. The estimated volume

was 0.036 m^3 (1.28 ft^3). To minimize the suspended weight, the mannequin was constructed from fiberglass molded from a full size mannequin provided by Armstrong Lab, AL/CFD. The mannequin was a 50th percentile size man 1.68 m (5.5 ft) tall with an inseam of 0.74 m (29 in). This size is slightly larger than normal for the size bicycle frame that was used. This again helped to simulate a track bicycle type configuration where in this form of racing the bicycle is usually sized smaller. The legs were molded into a pedal horizontal position. This position is one of two extreme pedal positions. It was chosen because it provided a case where one leg is at the extreme forward position and the other leg is at the extreme rear position. This is also the position that has been used in other testing [6]. The as installed bicycle and mannequin configuration is shown in Figures 7a and 7b.

AFIT 5-ft Wind Tunnel

This study utilized the AFIT 1.5 m (5 ft) wind tunnel located in Building 19, Wright-Patterson Air Force Base, Ohio. The wind tunnel is an open return type tunnel with a closed 1.5 m (5 ft) diameter test section. The total pressure provided by the tunnel is atmospheric thus dynamic pressure is the difference between tunnel static and atmosphere. Tunnel q is measured at the inlet of the test section averaged over 8 static ports located at the circumference at that location. The flow is generated by 2 sets of fans and associated motors. For this test, only one fan and motor set was required to provided the 40 - 56 km/h (25-35 mph) speed range. The tunnel performance was evaluated for this extremely low-speed range and the results are provided in Section VI.

The building in which the wind tunnel is housed has significant 60 Hz noise on the a/c ground. Considerable effort was expended to reduce this noise that is present on all measurements. Initially, the noise level was approximately 100 mV peak to peak. After

rearranging the instrumentation rack and patch panel ground path and moving the actual ground cable from a metal fixture to the a/c ground, the noise was reduced to 10 mV peak to peak. Operating the data acquisition system in differential mode, where each measurement channel is provided a reference voltage, proved to be the most effective noise reduction. The current noise level is 0.4 mV peak to peak.

IV. EXPERIMENTAL PROCEDURE

Calibration

For the commercial balance, calibration was achieved by mounting a calibration fixture on the balance then loading this fixture with known weights. Loading was isolated into each of the primary directions while recording the resulting output voltage of all six gages to determine the primary calibration curve as well as any coupling between the gages in the balance. Each direction was loaded in a positive and negative direction except axial which is only calibrated in the positive direction. Once the data was recorded, a calibration matrix is formed according to

$$\{\mathrm{v}\} = [\mathbf{C}]\{\mathrm{w}\} \tag{4}$$

where v is the six by one measured voltage vector, **C** is the six by six calibration matrix, and w is the six by one applied weight vector. The calibration matrix is determined from a least squares fit to the voltage data. Ideally the correlation of the data with the least squares fit should be 1.0. The principle elements of the calibration matrix, i.e., **C**11, **C**22, and **C**33, etc., had correlation coefficients of 0.999.

The single component balance was calibrated similarly. However in this case with only the single component, the calibration matrix is simply a single equation represented by the equation of a line

$$\mathrm{v}_{\mathrm{norm}} = \frac{\mathrm{v}_{\mathrm{meas}}}{e_i} = m_{\mathrm{norm}}\mathrm{w} + b_{\mathrm{norm}}$$

where v_{norm} is excitation normalized voltage measured from the Wheatstone bridge due to the applied weight w and m_{norm} and b_{norm} are coefficients from a least squares curve fit to the data. Since the strain gage output is a function of the voltage applied to the bridge, the output voltage was normalized by this input excitation such that the units of the slope are 1/N (1/lb_f) and the intercept is nondimensional. The correlation coefficients for the single component balances were 0.99999. This gave the indication that the flexure material, size, strain gages and adhesive were working correctly to provide a good transducer. Check loads were within 0.022 N (0.005lb_f).

Testing

Cylinder Configuration

The cylinder drag data was collected with both the commercial six-component balance and the single component balance. The new data acquisition card and software were used for both configurations. Before each test run, a quiescent data point was taken. It is this zero data point that is subtracted from all the data in the reduction routines to reference the data to a known condition. A run consisted of collecting data at velocities of 40, 48, and 56 km/h (20, 30, and 40 mph). Angle of attack was maintained at zero and no configuration changes were made to this model. Time history and averaged data were taken for a total of 1 second at a rate of 2400 Hz. The sampling time and rate were chosen to ensure a consistent average due to vibrations the model produced during testing. Likewise, at these rates the 60 cycle noise would also average out.

Bicycle Configuration

For this phase of testing, only the special single component balance was used. Like the cylinder testing, data was collected for the discrete velocities of 40, 48, and 56

km/h (20, 30 and 40 mph) for each configuration with a zero taken before each run to reference the data. There were considerable vibrations encountered during these runs due to the weight of the bicycle suspended vertically and the spinning wheels. The data was therefore collected for a longer period of time to ensure an acceptable average was obtained. The sampling rate was reduced to decrease the size of the resulting time history. Spinning and static wheel data was collected during these runs with the wheel rpm's matched to the tunnel speed. Data was collected for six spacings that ranged from the minimum the bottom bracket and crank width would allow to a total maximum of .25 m (10 in) wide. In addition, two narrower spacings were achieved by slightly reconfiguring the mannequin. These positions were not considered pedaling positions since the frame would interfere during the pedaling stroke. They are better compared to hill descent positions where the rider is tucked into the frame as close as possible. The entire spacing range was completed on the open frame first then repeated for the enclosed aerodynamic frame. Static and spinning rear wheel effects were investigated for each frame. The front wheel was static in all cases. This was a compromise in simulating the real world but as the results will show the windage of the rotating wheels had little effect on the overall trends.

V. DATA REDUCTION

Wind Tunnel Corrections

The raw voltage data were reduced in the Lab VIEW software following the format of the prior WIND software. The data was converted to engineering units via their associated calibration curves. Based on the recommendations found in Pope [15], corrections to tunnel dynamic pressure (q) for solid and wake blockage (sb and wb) and skewness were applied to the data according to

$$sb = \frac{k_1 V_{\text{model}}}{A_{\text{tunnel}}^{1.5}}$$

$$wb = \frac{\text{drag}}{4 q_{meas} A_{\text{tunnel}}}$$

where k_1 is a model shape factor, V_{model} is the model volume and A_{tunnel} is the tunnel area. These corrections combine into

$$q_{\text{corr}} = q_{meas} k_2 (1 + sb + wb)^2$$

where k_2 is the skewness factor, all of which results in a total correction to q.

Several corrections to the measured drag data were also required. A buoyancy correction to the drag data in the form of

$$D_b = -\frac{\Delta_p}{\Delta_l} V_{\text{model}}$$

where V is the volume of the model and Δ_p and Δ_l were previously determined for the tunnel, was applied. An additional correction was necessary for the vertical system due to the drag from the sting connecting the model to the flexure. Because of this unique arrangement, the drag on the sting could not be measured directly, therefore an estimated drag reduction was applied equal to

$$D_s = qC_d A_{\text{sting}}$$

where q is the tunnel dynamic pressure, C_d was equal to 1.0 and A_{sting} was the projected frontal area of the sting.

The relative size of these corrections for a typical cylinder data set is provided in Table 4. These corrections are based primarily on the geometry of the model and tunnel characteristics except for wake blockage, which also depends on measured axial force.

Table 4. Summary of Cylinder Data Corrections

q_{meas}, Pa (psf)	q_{corr}, Pa (psf)	sb	wb	Drag, N (lb_f)	D_b, N (lb_f)	D_S, N (lb_f)
33.52 (0.70)	34.47 (0.72)	2.82e-3	9.83e-3	2.05 (0.46)	-0.37 (-0.084)	-0.26 (-0.059)
78.04 (1.63)	79.96 (1.67)	2.82e-3	9.41e-3	4.98 (1.12)	-0.37 (-0.084)	-0.62 (-0.14)
110.60 (2.31)	113.00 (2.36)	2.82e-3	9.23e-3	7.12 (1.60)	-0.37 (-0.084)	-0.85 (-0.19)

These corrections were also applied to the bicycle data based on an estimate of the mannequin and bicycle frontal area and volume. However, due to the unusual shape of the model, it is perhaps more appropriate to present changes in drag relative to a baseline configuration such that these corrections cancel out. By doing so, the error in the measurement of drag reduces to the error in the strain gage measurements only and not in how accurately the area and volume are known. The baseline configuration will be the nominal spacing obtained using a standard crank set and 0.07 m (2.75 in) bottom bracket width.

VI. RESULTS

The results of this multi-phased project are presented in the following sections in the order in which they were accomplished. The successful completion of each phase allowed the build up of the capability to accomplish the primary testing. Where appropriate, a complimentary set of English unit plots is provide in Appendix B.

Wind Tunnel Low-speed Capabilities

Static and dynamic pressure measurements were used to evaluate the capabilities of the wind tunnel in the racing bicycle speed regime of 32-64 km/h (20-40 mph). A concern existed initially that at these low speeds the flow through the tunnel would not completely fill the test section. As a result, 25 static wall pressures were taken at the stations specified in Figure 2 to determine if the pressures were uniform not only at the tunnel cross section but also streamwise down the tunnel. (Note that port 13 was deleted because the port was unknowingly plugged during the testing. In addition, port number 26 is located upstream as shown in Figure 2.)

The pressures, summarized in Figure 8 for test speeds of 32, 48, and 64 km/h (20, 30 and 40 mph), are presented as differential pressures relative to a reference pressure, which in this case was ambient. These pressures were accurate to 3.44 N/m^2 (0.0005 psid) as characterized by the manufacturer. The negative values of the data results from the tunnel operating at a pressure less than ambient. As seen in the figure, the pressures are uniform, varying only 6.89 N/m^2 (0.001 psid) for the 32 km/h (20 mph) case at all locations. For the remaining two test velocities, the pressures are uniform from port 1 to port 14 which covers the majority of the test section. Variations in the pressures that begin at ports 15, 16, 20, and 24 are due to obstructions and irregularities in the tunnel

walls at those locations. This data was taken with the model mounting yoke and apparatus installed within the test section.

Additional time history data, collected from a ring of static ports at the tunnel inlet where tunnel q is determined, was collected to see how steady the flow was. The data shows further that the tunnel provides adequate flow but also brings to light some interesting characteristics of the tunnel. Figures 9, 10, and 11 present for 40, 48, and 56 km/h (25, 30, and 35 mph), respectively, a comparison of time history q data for cases where the tunnel was operated with the rear fan only or the front fan only with the flow straightner screen in and out of position. The variations, as represented by the standard deviation, in dynamic pressure were smaller when the tunnel was operated with the rear fan and motor set. The difference in performance between the front and rear fans is likely due to their physical locations in the tunnel. The front fan is positioned 8.2 m (27 ft) upstream of the exit and must force the air passed the motors and drive shaft tunnel whereas the rear motor is located near the exit plane. Even more surprising is the fact that the front fan is missing two blades. Sometime during the life of the tunnel a blade must have become damaged and removed with the other opposite blade removed for balance. Based on the above, the subsequent drag tests were performed with the rear motor and fan set.

Evaluation of the above data shows that AFIT 1.5 m (5ft) wind tunnel is capable of operating in the 32-64 km/h (20-40 mph) speed range. The static pressures are uniform at stations along a majority of the test section precluding the existence of any voids in the flow. When the rear fan and motor set are used a steady flow is also obtained.

Three-Dimensional Cylinder Drag

The results for the aerodynamic drag of a three-dimensional cylinder are presented first for the six-component balance and then the single component balance. The six-component balance was initially investigated to determine if it could be used in the low force regime. It was also used as a comparison for the single component balance. The aerodynamic drag was then measured with the single component balance to verify it was capable of accurate and repeatable measurements. Repeatability checks were performed for both balances. The accuracy of each system was determined from the methodology supplied in Appendix A. Finally, the data for both balances are compared to other experimental results.

Commercial Six-component Balance Results. Using the six-component balance, the aerodynamic drag from the three-dimensional cylinder model was measured at the discrete velocities of 32, 48, and 64 km/h (20, 30, and 40 mph) to obtain the variation of drag with tunnel dynamic pressure. The results for the total drag of the cylinder (corrected as described in Section V) are plotted against q for two separate runs in Figure 12. The repeated case was run the following day to allow the induced flow in the tunnel building to settle and the tunnel motors to come to a complete stop. The data in both cases varies linearly with dynamic pressure, as expected, giving a value of nearly 12.2 N (2.75 lb_f) at 64 km/h (40 mph). A least squares curve, fit through the combined data, is included in the plot and has a correlation coefficient of 0.99999. The figure also shows the repeatability of the measurements with the data points nearly overlaying each other. The repeatability of the data was determined by subtracting the two runs from each other and reporting the worst case magnitude. The results of the repeatability check were instrumental in assessing the validity of the initial results as well as the impact of the dynamics of the

system on the measurements. For these data sets, the repeatability was 0.048 N (0.011 lb_f) at 32 km/h (20 mph) which gives the indication that the measurements and procedures were correct. Likewise, this shows that the sampling rates have effectively captured the average of the data despite the vibrations of the system.

However, when the data is compared to other experimental results, greater differences are apparent. Hoerner [14] provides a summary of experimentally determined drag coefficients for cylinders of various height to span ratios. According to this reference, the resulting C_D, for the cylinder used in this study with a height to span ratio of 0.21 should have been equal to 0.75 at a Reynolds number of 10^5. The measured C_D, for the same Reynolds number, was 0.82 which corresponds to a 9% difference. Figure 13 presents a comparison of the six component drag data and the computed results for a C_D of 0.75 at the test dynamic pressures. The measured results are consistently higher than expected with Figure 14 showing variations as much as 1.11 N (0.25 lb_f) at 64 km/h (40 mph) between measured and expected values for the two cases . The differences appear as a linear offset which is likely due to the resolution of the balance. Even though the use of the commercial balance in this extremely low load range may be exceeding its capabilities (realizing the commercial balance was designed for a full scale axial load of 222.41 N (50 lb_f)) the data provided a comparison for the new acquisition software and single component balance.

Single Component Balance Results. The drag on the three-dimensional cylinder was then measured using the single component balance. The data was collected for a slightly different velocity range of 32, 40, 48, and 56 km/h (20, 25, 30, and 35 mph) to completely evaluate the new system. Again several runs were made to ensure repeatable data. The measured total drag (corrected as described in Section V) is plotted versus dynamic

pressure in Figure 15. The drag varies linearly with q having a least squares curve fit correlation coefficient of 0.9998. The results were repeatable to within 0.089 N (0.02 lb_f). This variation in the data was greater for the single component balance than that found using the six-component balance and was not totally unexpected considering the greater amount of vibration that was observed when using the single component balance. The increased vibration is attributable to the vertical arrangement and the thin flexure that was required to measure the small changes in drag. The resulting system dynamics were equated to that of a pendulum where the model weight acts like the bob of a pendulum and the connecting sting like the pendulum rod. The slight variations in the flow coupled with the vortices shed from the model acted as a sinusoidal forcing function with the typical result shown in Figure 16. Although similar oscillations were also present in the commercial balance, the pendulum arrangement of the vertical system resulted in variations as much as 1.11 N (0.25 lb_f). Clearly however, the oscillations occurred around a mean value. As a result, sampling rates for the single component balance were adjusted to capture several oscillations such that a consistent average in the data was obtained.

The single component results were compared to the $C_D = 0.75$ case as well. In contrast to the commercial balance, the results, shown in Figure 17, are consistently lower but overall compare more favorably. The measured C_D was 0.72 which is a 4% difference compared to the $C_D = 0.75$ results. The differences in the measured and expected values were between 0.22 and 0.44 N (0.06 and 0.10 lb_f) (see Figure 18). These differences are larger than the estimated error for this system (see Appendix A). The uncertainty in the these results lies not in the drag measurement but more likely with the estimate for the tare drag of the sting that connects the model to the balance. The estimate was based on the assumption that the sting was idealized as a two-dimensional cylinder with a C_d equal to 1.0. This a conservative estimate, since in actuality the sting tapers at one end and has a

1.0. This a conservative estimate, since in actuality the sting tapers at one end and has a nearly flat side on the other end. The end effects would likely reduce the drag compared to a two-dimensional case [14].

The above results show the new vertical system and single component balance was able to measure the drag on a three-dimensional cylinder to within 0.44 (0.10 lb_f) when compare to other experimental results. In addition, the results from the new system compare to a better degree than the six-component balance. The estimated error based on a typical single-component data set was 0.05 N (0.012 lb_f) which also indicated the new system was adequate for the measurement requirements of the primary bicycle testing.

Bicycle/Rider Low Drag Configurations

Preliminary Results. Before the primary testing began, the drag for several bicycle configurations was measured to obtain results in which to compare to previous research. Initially, the bicycle was configured as described in Section III but with conventional 0.69 m (27 in) spoked wheels instead of the aerodynamic wheels. The mannequin was not installed. The resulting drag at 48 km/h (30 mph) was 10.81 N (2.43 lb_f) which compares to 10.63 N (2.39 lb_f) obtained previously [1] for a similar bicycle configuration. The drag for a skirted aerodynamic wheel was also determined. The new system measured the drag to be 1.47 (0.33 lb_f) which again compares to 1.33 N (0.30 lb_f) [3].

General Results. As in the cylinder testing, data was collected at discrete velocities for 8 predetermined spacing of the rider's legs. The process was then repeated over the entire spacing range to show repeatability of the measurements. Although total drag values are

drag because the total drag is for a half-mannequin system for which there is no other data to compare. Differencing the data to obtain changes relative to the standard spacing at 0.11 m (4.25 in) provided a means to compare the data to one another and establish trends. In addition, the unwanted drag from the sting, and cables for the rpm sensor and wheel spin motor, as well as, the buoyancy corrections are removed from the data.

An example of a typical test data set is shown in Figure 19 for two separate runs. Like the cylinder testing, a least squares curve is fit to the data with the data points nearly overlaying each other. On the basis of the experience from the cylinder testing, the sampling time for the data was increased to ensure the repeatability of the measurements. In the case of the bicycle and rider model, Figure 20 shows a typical drag force time history where the oscillations vary as much as 2.22 N (0.5 lb_f). Although they occur around a mean value, the oscillations are not strictly sinusoidal (as they were for the cylinder). The complex interaction of the mannequin and rider wakes in conjunction with the "pendulum effect" of the vertical system is evident in this figure. With the dynamics as they were, the worst case repeatability (calculated as before) of the measurement was typically 0.076 N (0.017 lb_f).

Open Frame Configuration Results. Spacing variation data was collected for the open frame configuration with the rear wheel spinning. Recall that the front wheel was static in all cases. A comparison of the total drag versus the spacing parameter, s, for the test velocities of 40, 48, and 56 km/h (25, 30, and 35 mph) is summarized in Figure 21. (Recall from Figure 4 that s is the spacing between the crank arms or essentially the total spacing between the rider's feet as s is increased.). The trend of the data is surprisingly linear. As the figure shows, the most streamlined position, which occurred at the narrowest spacing of 0.03 m (1.125 in), achieved the lowest drag. Recall however, the

two smallest spacings required the mannequin to be slightly repositioned. These positions would be considered hill descent positions based on the 0.07 m (2.75 in) bottom bracket used in this testing. With this in mind, the standard spacing for the open frame configuration is the best spacing to achieve the lowest drag. As a reference point, the standard spacing is located at 0.11 m (4.25 in) as indicated by the dashed vertical line in all the figures. Although the curves in Figure 21 are relatively flat and appear insensitive to changes in spacing, the following plots will show the changes in drag are substantial considering the low power of bicycle and rider system.

The changes in drag were obtained by subtracting the drag value at the standard spacing (s = 0.11 m (4.25 in)) from the drag at the other spacings for speeds of 40, 48, and 56 km/h (25, 30, and 35 mph). (In all the following plots, a vertical line at the standard spacing is provided as a reference.) At 40 km/h (25 mph), Figure 22, the trend appears somewhat linear but is not as well behaved as will be shown for the other test speeds. In general, the results for the 40 km/h (25 mph) runs, for both open and closed frame/spinning and static wheels, exhibit greater variation in the data than at the higher speeds. This is again is attributable to the vertical arrangement of the sting where the oscillations at the lower speed were greater and less damped than the higher speeds. Referring again to Figure 22, the results show that narrowing the spacing 0.08 m (3 in) from standard would provide a 1.11 N (0.25 lb_f) reduction in drag or almost a 0.7 sec time advantage for a 1000 m time trial. There is little change in drag from s = 0.11 to 0.16 m (s = 4.25 to 6.25 in) indicating that any spacing in this range would yield acceptable drag levels and allow the rider to choose their most comfortable position within this range. Unfortunately, the results from the 48 and 56 km/h tests will show this not to be the case.

The results for the 48 and 56 km/h runs, shown in Figures 23 and 24 respectively, clearly show a linearly decreasing trend in drag with decreasing spacing. The relative difference between the narrowest to widest spacing is nearly 2.67 N (0.6 lb_f) in both cases which shows the substantial impact the rider can have on the drag of the system. Interestingly, the relative change from the standard to narrowest spacing is still near 1.11 N (0.25 lb_f) for both runs as was the case for the 40km/h results. The insensitivity to spacing change observed at 40 km/h (25 mph) is not present in either Figure 23 or 24. The difference in drag between the spacings at 0.11 and 0.16 m (4.25 and 6.25 in) is now a significant 0.8 N (0.18 lb_f) for both cases.

The results for the 48 and 56 km/h (30 and 35 mph) (Figure 23 and 24) speeds show the linear trend that was observed in the total drag data (Figure 21). However, a deviation in the trend is visible at s = 0.21 m (8.25 in). The difference is slight and is nearly within the error of the measurement. (The width of the plotting symbol is approximately the error.) The data is the average of several points and is repeatable. This deviation persists in several of the following cases and is therefore believed to be real.

As shown in Figure 25, the linear effect of the spacing on total drag persists even in the case where the rear wheel is static. Likewise, the change in drag at the various test speeds shown in Figures 26, 27, and 28, is nearly linear in all cases. The spacing at 0.69 (8.25 in) is the exception to the trend where the deviation is nearly 0.98 N (0.22 lb_f). Even with this outlier, the conclusion to streamline to reduce drag is unaffected.

Closed Frame Configuration Results. The spacing variation tests were then repeated for the closed frame bicycle configuration. Figure 29 presents the effect of the spacing on the total drag for the rotating wheel case. When compared to the open frame, the closed

(aerodynamic) frame has a lower drag of 1.11 N (0.25 lb_f) at the standard spacing. The linearly decreasing trend of the drag with decreasing spacing that was visible in the open frame configuration is not present in the closed frame results. The shape of the trend has changed subtly to reveal the effects of the splitter plate arrangement formed by the closed frame and disk wheel.

Differencing the data more readily shows the splitter plate effect trend. Although decreasing with decreasing spacing, the drag trend for the 40 km/h speed shown in Figure 30 is somewhat vague. The results show an insensitivity to changes in spacing from 0.07 to 0.16 m (2.75 to 6.25 in). The results for the higher speeds, Figures 31 and 32, clearly show a higher-order curve with a local minimum value. It is this local minimum that is suggested by splitter plate theory. Even though the narrowest spacing at 0.03 m (1.25 in) still provides the lowest overall drag, slightly narrowing the spacing from standard would now cause an increase in drag of nearly 0.44 N (0.10 lb_f) for both the 48 and 56 km/h (30 and 35 mph) cases. This is in contrast to the open frame configuration where any decrease in spacing would decrease the drag. Like wise, a slight increase in the spacing results in a increase in drag of 0.44 N (0.10 lb_f). To the rider, an increase in drag of this magnitude translates to a 1.22 sec or 15 m (49 ft) deficit at the finish line of a 4000m race.

The drag also appears to reach a plateau or local maximum at the 0.21 - 0.23 m (8.25 - 9.25 in) spacings indicating the wake from the legs of the rider is reattaching past the splitter plate. When this occurs, the splitter plate is unable to affect the wake and the drag increases.

These trends persist when the rear wheel was fixed. The total drag results summarized in Figure 33 shows the standard spacing provides the minimum drag

configuration. Figure 34 shows the effect of spacing on the change in drag at 40 km/h (25 mph). The results are do not show a linear trend as was the case for the open frame configuration but the splitter plate trend is not clearly visible either. At the higher speeds, the splitter plate effect is more prominent with the standard spacing at 0.11 m (4.25 in) providing the minimum drag (see Figures 35 and 36).

VII. CONCLUSIONS

1. The tunnel is capable of providing uniform and steady flow for the low-speed regime of 40-56 km/h (20-40 mph). The lowest achievable velocity, limited only by the motor switching and control hardware, was 27 km/h (17 mph). A flow with less variation in static and dynamic pressure is obtained when the rear most fan and motor set is used.

2. The low force measurement system developed for this thesis was shown to be capable of repeatable and accurate measurements. The estimated error of the force measurement was 0.05 N (0.012 lb_f) based on a typical data set and was more than adequate for the testing. The system expands the capabilities of the AFIT 1.5 m (5 ft) wind tunnel, enabling further development testing in other low force studies that were previously discouraged due to lack of capabilities.

3. For the open frame bicycle and rider configuration, the drag decreases linearly with decreasing spacing. The lowest riding drag configuration using this frame, for both static and rotating rear wheel, was the standard spacing. The splitter plate effect was not apparent in the trend and there does not appear to be a minimum spacing as theory might suggest. The conventional wisdom to streamline the rider to the bicycle prevails. Use of a larger diameter disk wheel in the rear may enhance the splitter plate effects for an open frame configuration.

4. Converting the model to a closed frame enhanced the splitter plate effects of the system as was hypothesized by this study. The overall trend shows a lower drag configuration would exist at a spacing other than the absolute minimum. The lowest drag was at the

nominal spacing for both rotating and static wheel cases. Combining the results of both configurations would indicate that by reducing the bottom bracket width of the bicycle frame would reduce the drag of the system. In addition, a weight savings would be realized as well. If the resulting frame is an open frame configuration further drag reduction could be achieved through narrowing the frame and rider spacing. If the frame used is a closed type frame then caution must be used in reducing this spacing further or an increase in drag could result,

VIII. RECOMENDATIONS

1. For the open frame model, an absolute minimum drag configuration was not found due to the hardware limitation of the bicycle used. The spacing evaluation should be repeated for a frame with a smaller bottom bracket to determine if an absolute minimum exists. In addition, a larger diameter rear disk wheel could be tested to try to enhance the splitter plate effect. Although limited by other performance factors and possibly the ICF rules, the wheel base of the frame could be varied to determine if this impacts the splitter plate effect of the aerodynamic frame and disk wheel.

2. Additional rider leg positions should also be completed to ensure the trend found in this study persists. Likewise the variations should then be repeated to determine the trends when the model is yawed relative to the free stream to simulate a side wind. This test would require the following modification to the measurement system.

3. Based on the basic concept developed in this study, the vertical system and single component balance could be enhanced. The single component flexure should be expanded to include the measurement of side force by the addition of strain gages on the side of the flexure beam or by the addition of another beam oriented 90 degrees from the axial beam. This modification would allow testing of the model at a yaw angle to simulate a side wind.

REFERENCES

1. Burke, Edmund and Chester R. Kyle. "Improving the Racing Bicycle," Mechanical Engineering: 34-45 (September 1984).

2. Gross, Albert C., Chester R. Kyle, and Douglas J. Malewicki. "The Aerodynamics of Human-powered Land Vehicles," Scientific American, 249: 142-152 (December 1983)

3. Kyle, Chester R. "Wind Tunnel Tests of Bicycle Wheels and Helmets," Cycling Science: 27-30 (March 1990).

4. Hooker, Gary and David Spangler. "Scientific Performance Testing," Cycling Science: 2-5 (December 1989).

5. Hopkins, Mark W. and Frank S. Principie. "The DuPont Aerodynamic Bicycle Wheel," Cycling Science: 3-8 (March 1990).

6. Kyle, Chester R. "Wind Tunnel Tests of Aero Bicycles," Cycling Science: 57-61 (December 1991).

7. Lamb, David R. and Melvin H. Williams. Perspectives in Exercise Science and Sports Medicine. Ann Arbor, MI: Edwards Brothers, 1991.

8. Melton, Michael. Advanced Development Department, Huffy Corporation, Dayton, OH. Telephone Interview. 20 May 1994.

9. Mansingh, Vivek and P.H. Oosthuizen. "Effects of Splitter Plates on the Wake Flow Behind a Bluff Body," AIAA Journal: 778-783 (May 1990)

10. Zdravkovich, M.M. "Intermittent Flow Separation from Flat Plate Introduced by a Nearby Circular Cylinder," Flow Visualization II: 265-270 (1981).

11. Dally, James W., William F. Riley, and Kenneth G. McConnell. Instrumentation for Engineering Measurement. New York: John Wiley and Sons Inc., 1984.

12. Systems Research Laboratories. AFIT 5 Ft Wind Tunnel Data Acquisition System. Version 1.3, User's Manual. WPAFB, OH, April 1990.

13. Elledge, Alan, W. The Design and Development of a Low Speed, Low Force Wind Tunnel Data Acquisition System with an Application to Bicycle Front Fork Spacing. Unpublished thesis. Graduate School of Engineering, Air Force Institute of Technology (AU), Wright-Patterson AFB, OH, December 1994.

14. Hoerner, Sighard F. Fluid Dynamic Drag. Midland Park, New Jersey: Published by author, 1965.

15. Kyle, Chester R. Technical Director, Bicycle Aerodynamics Research, USCF, Telephone Interview. 10 May 1994.

16. Ray, William H. and Alan Pope. Low-speed Wind Tunnel Testing. New York: John Wiley and Sons Inc., 1984.

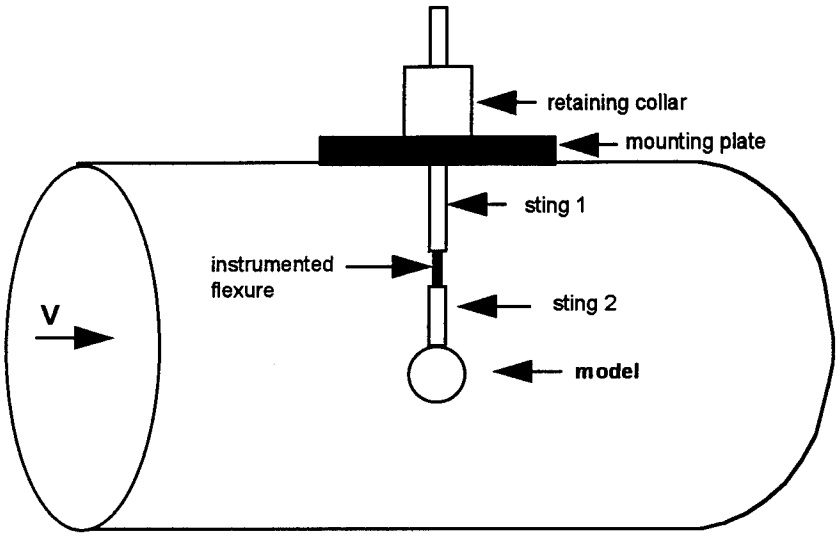

Figure 1. Vertical Model Mount Drag Measurement System

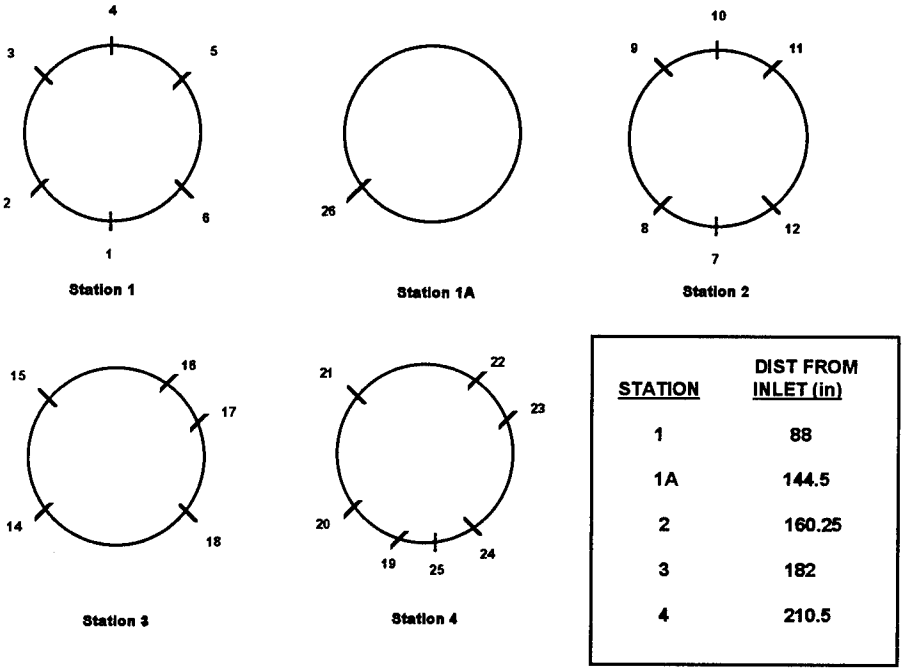

STATION	DIST FROM INLET (in)
1	88
1A	144.5
2	160.25
3	182
4	210.5

Figure 2. Static Pressure Port Tunnel Locations

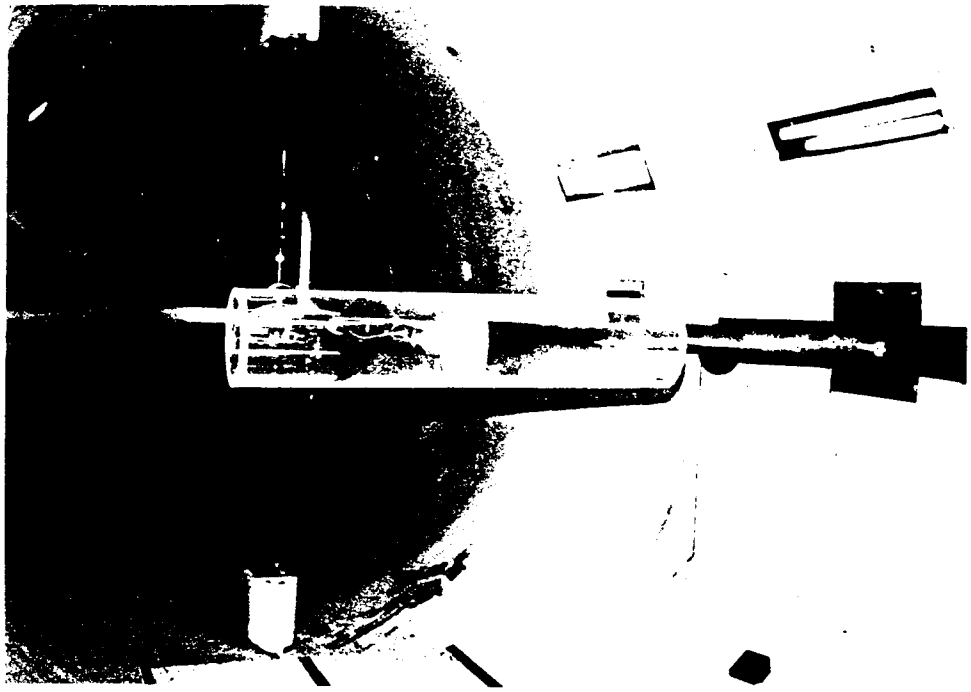

Figure 3a. Sting Mounted Cylinder Model Looking Downstream

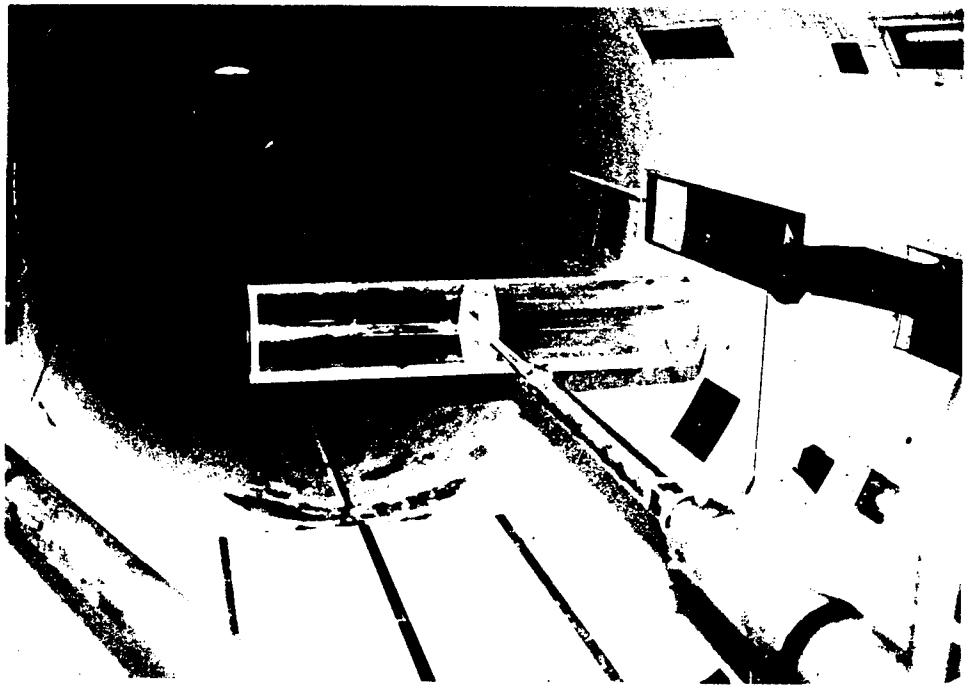

Figure 3b. Sting Mounted Cylinder Model, Looking Upstream

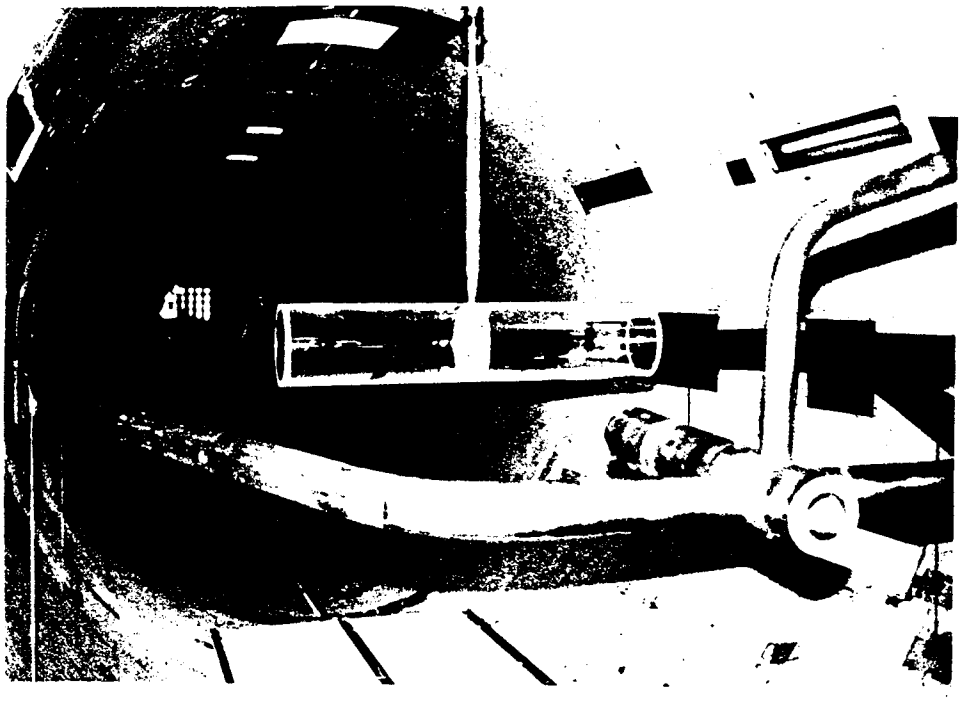

Figure 3c. Cylinder Model on Single Component Balance, Looking Upstream

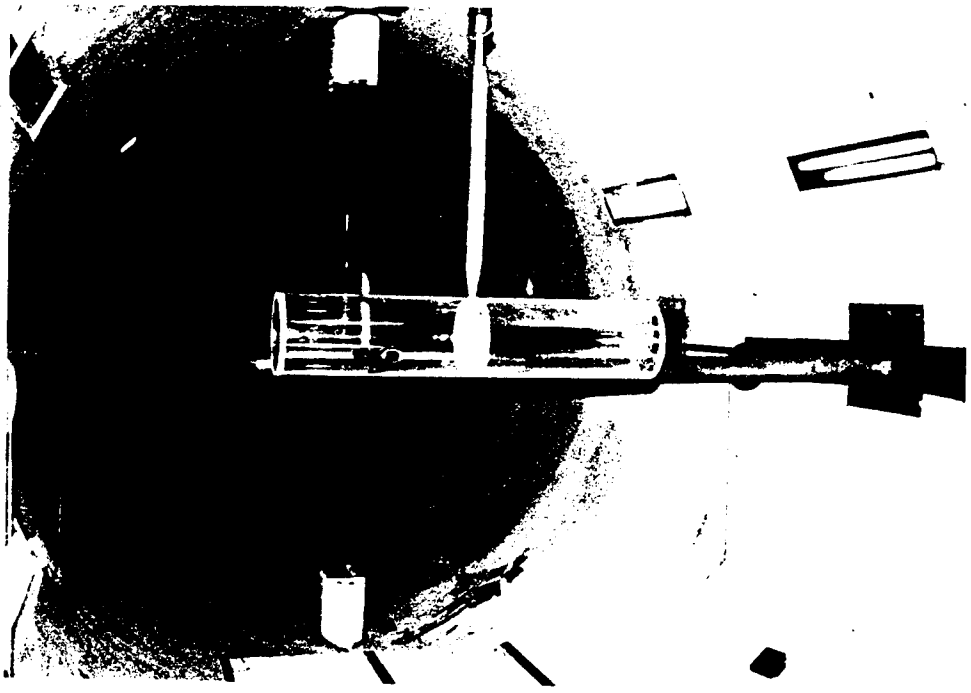

Figure 3d. Cylinder Model on Single Component Balance, Looking Downstream

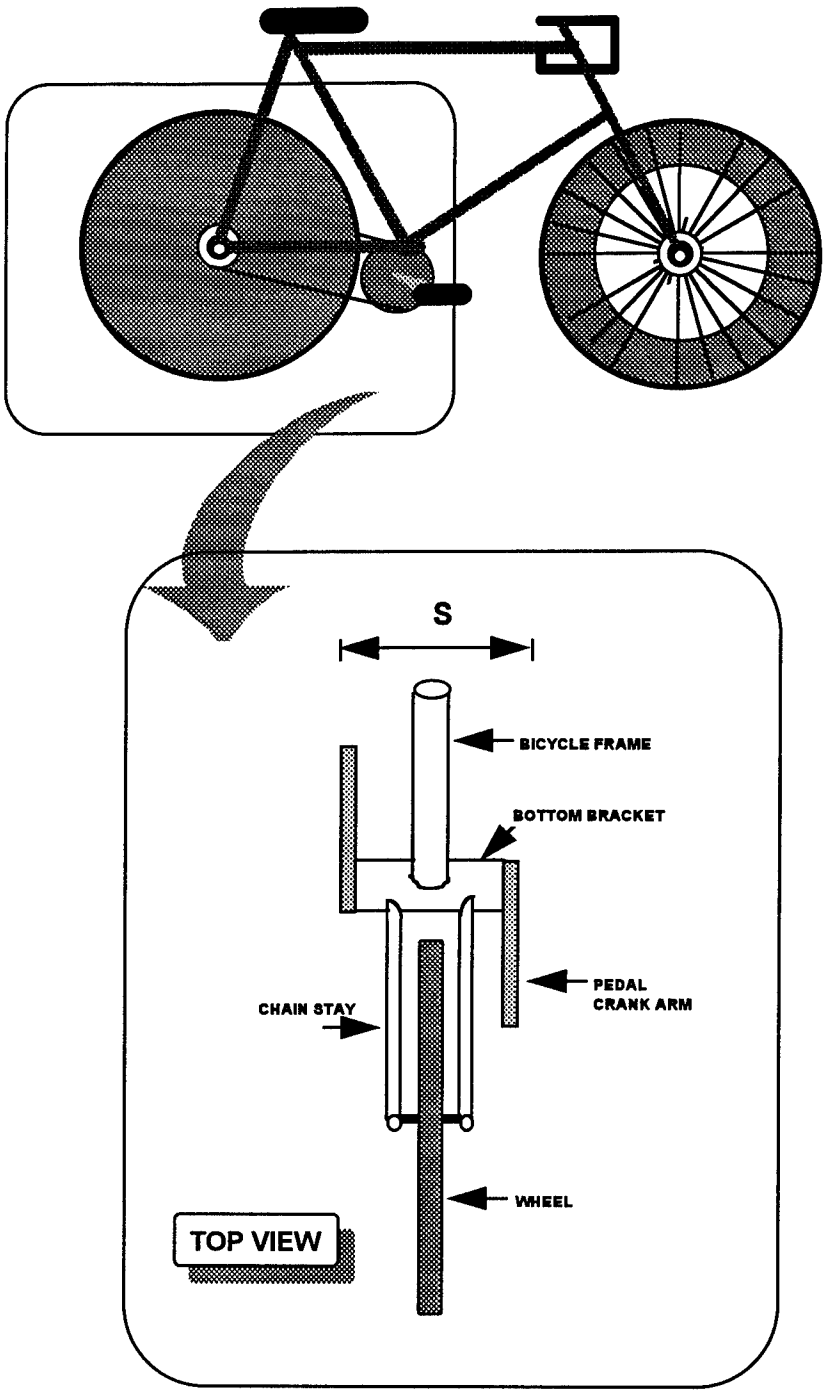

Figure 4. Illustration of Bicycle Spacing Parameter

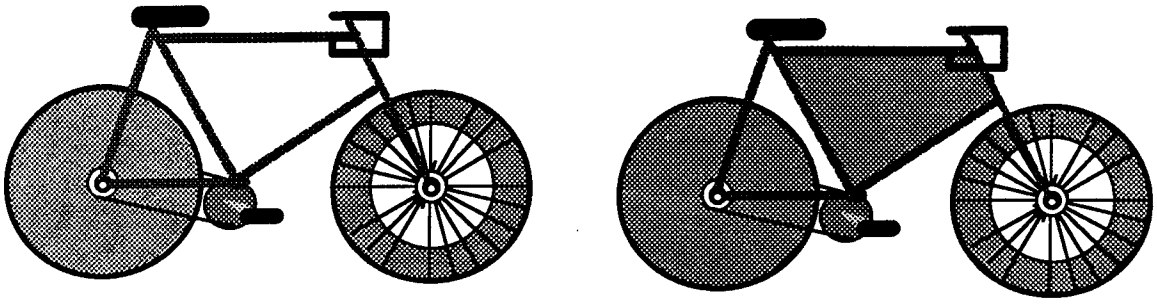

OPEN FRAME
CONFIGURATION

ENCLOSED FRAME
CONFIGURATION

Figure 5. Illustration of Frame Configurations

Figure 6. Disk Wheel

Figure 7a. Bicycle and Mannequin Configuration, Looking Upstream

Figure 7b. Bicycle and Mannequin Configuration, Looking Downstream

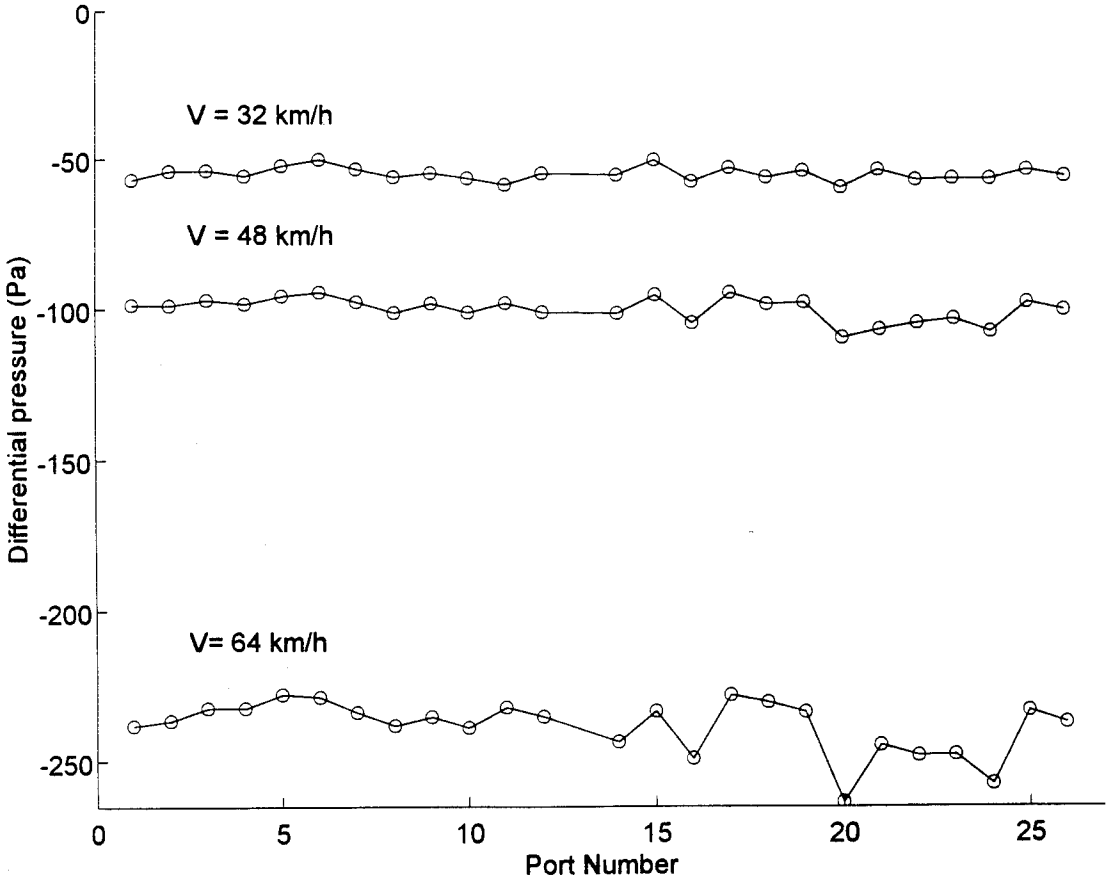

Figure 8. Wind Tunnel Static Pressure Distribution

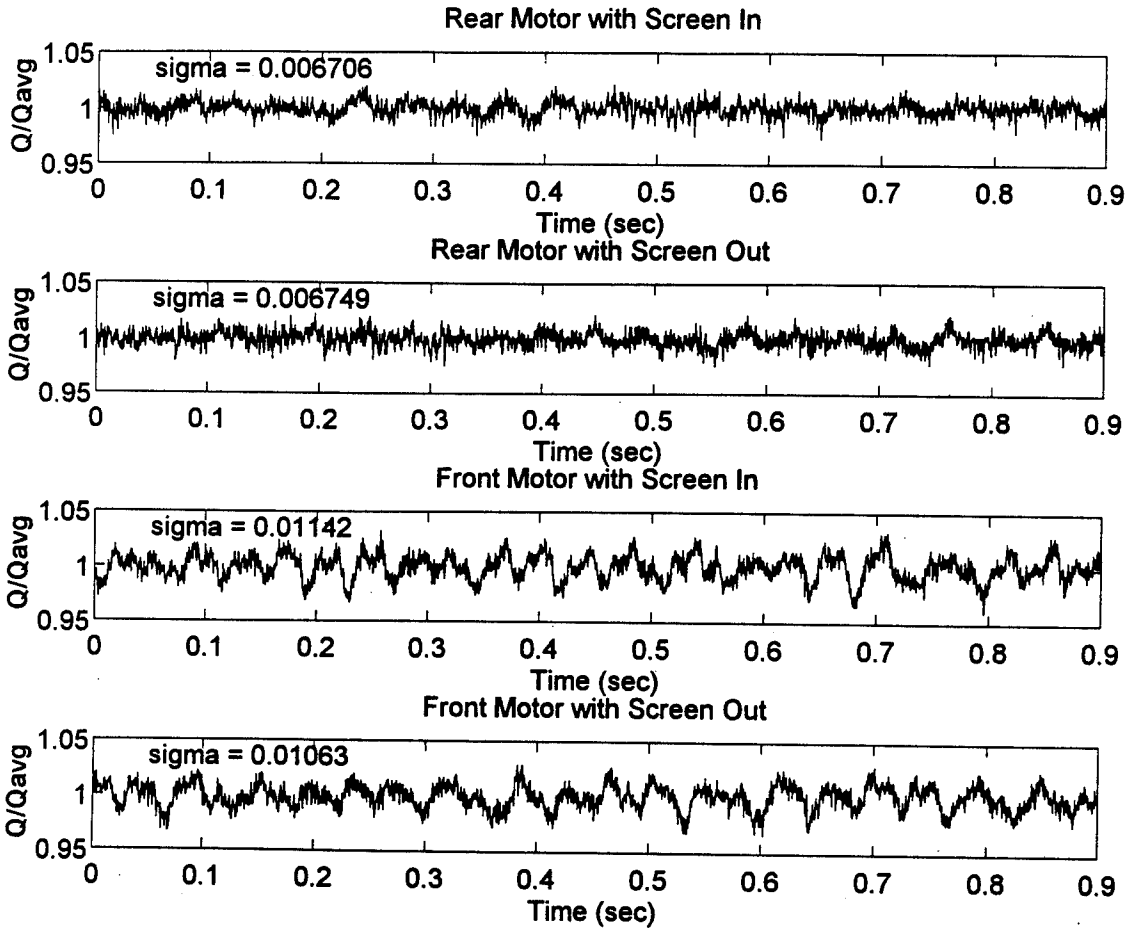

Figure 9. Effect of Wind Tunnel Motor on Dynamic Pressure, 40 km/h

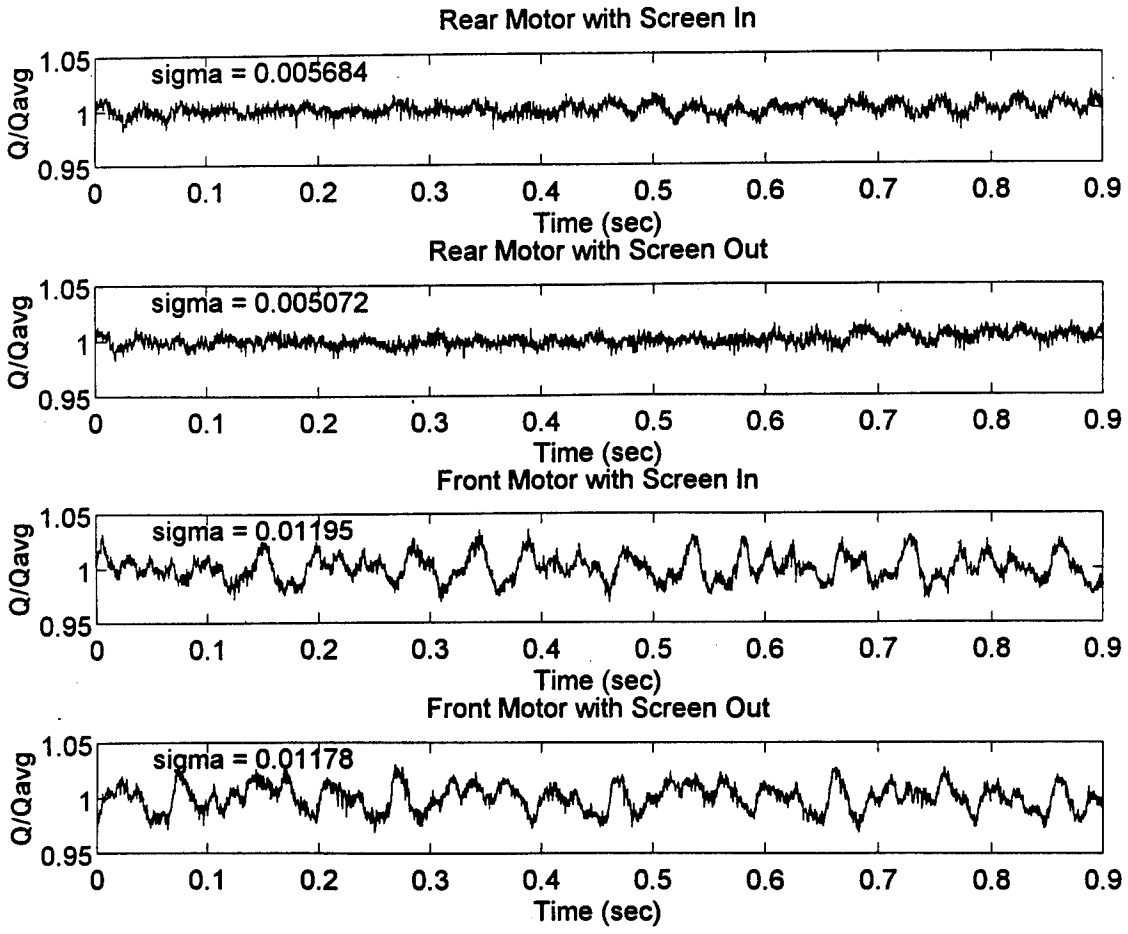

Figure 10. Effect of Wind Tunnel Motor on Dynamic Pressure, 48 km/h

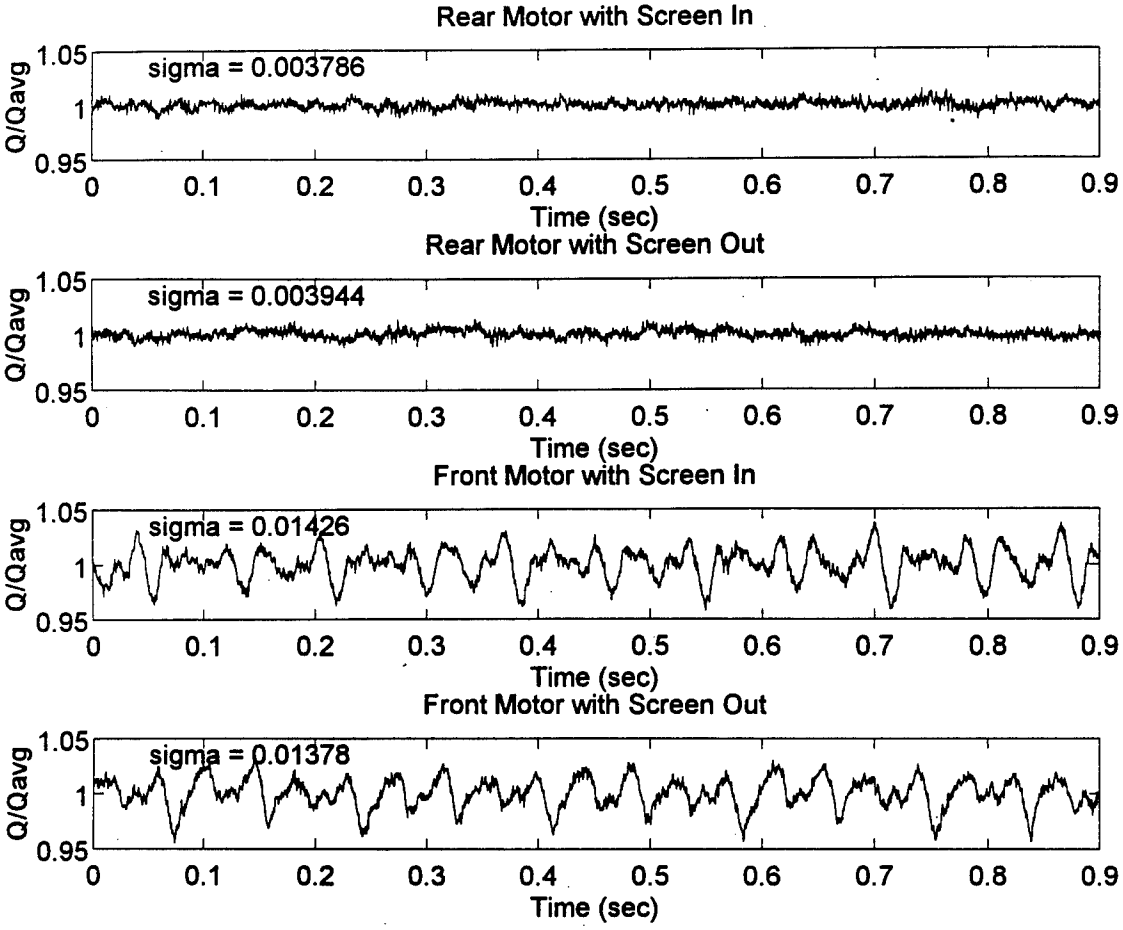

Figure 11. Effect of Wind Tunnel Motor on Dynamic Pressure, 56 km/h

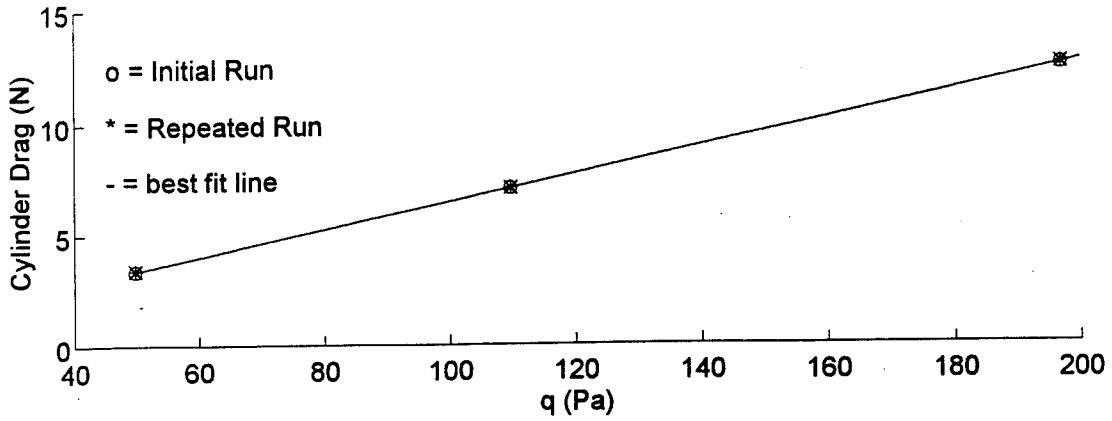

Figure 12. Repeatability Check, Six Component Balance

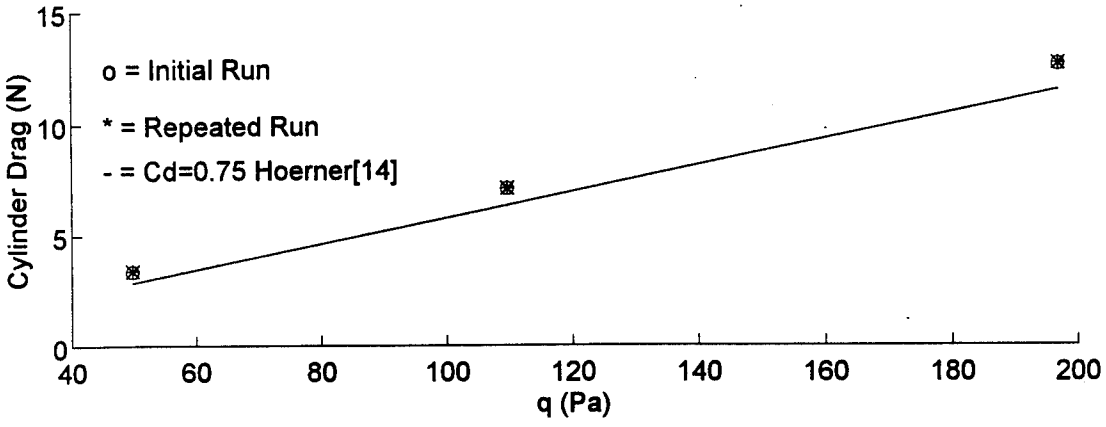

Figure 13. Comparison of Drag with Previous Results, Six Component Balance

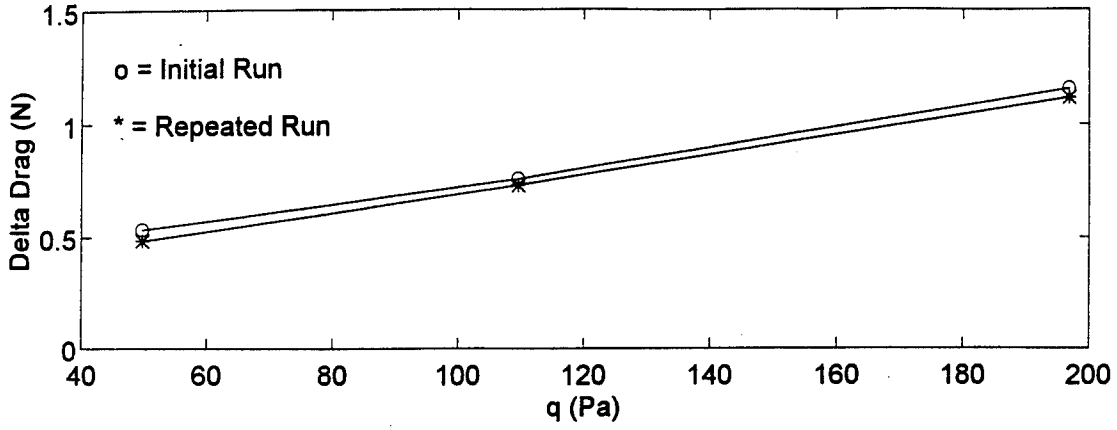

Figure 14. Difference in Drag with Previous Results, Six Component Balance

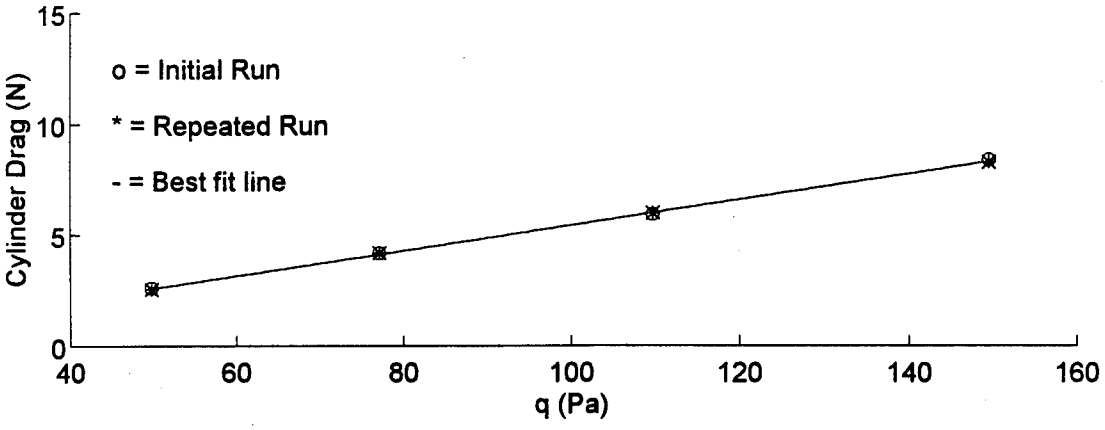

Figure 15. Repeatabilty Check, Single Component Balance

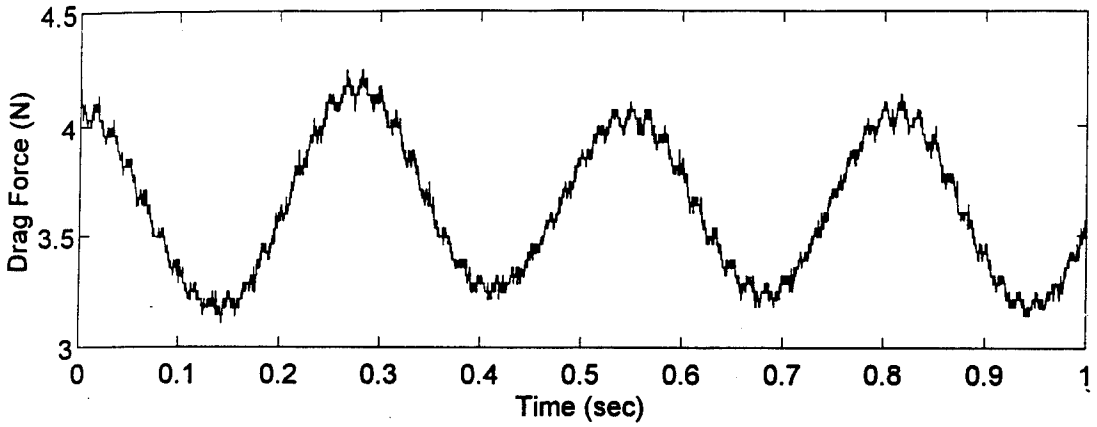

Figure 16. Variation of Drag with Time, Single Component Balance

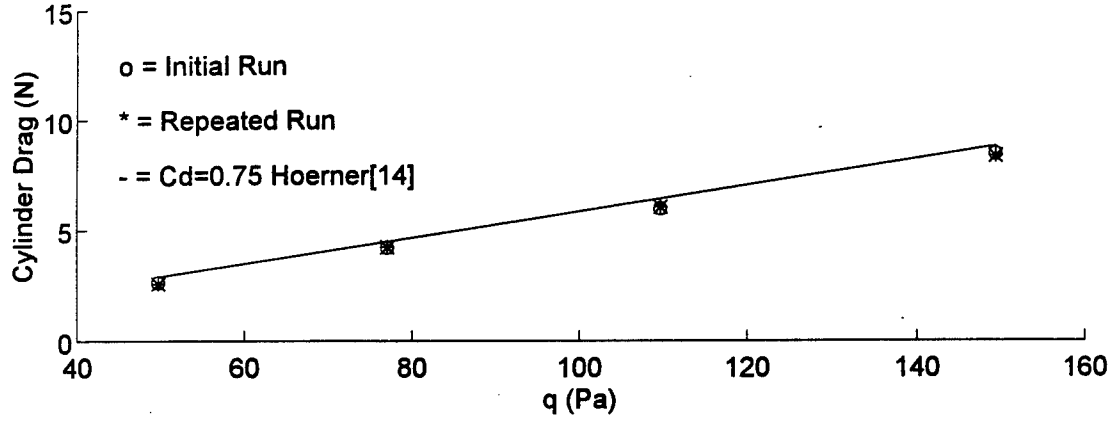

Figure 17. Comparison of Drag with Previous Results, Single Component Balance

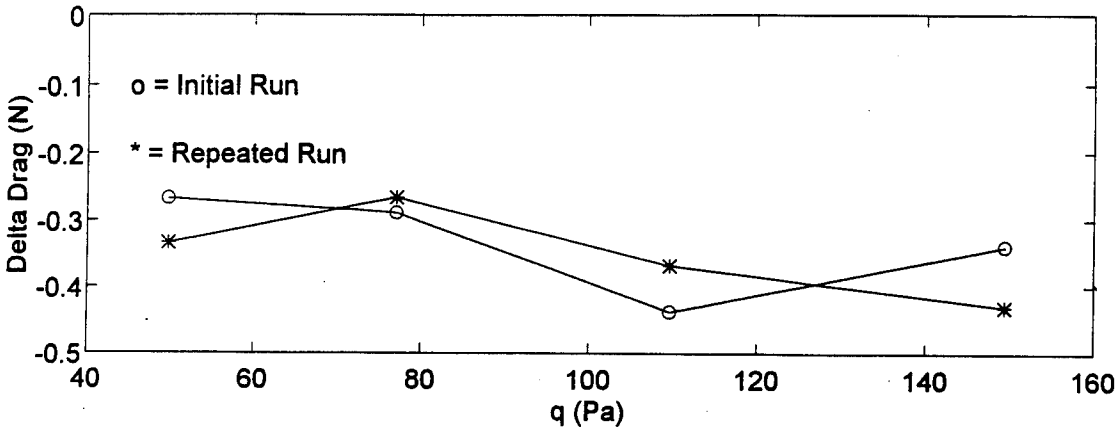

Figure 18. Difference in Drag with Previous Results, Single Component Balance

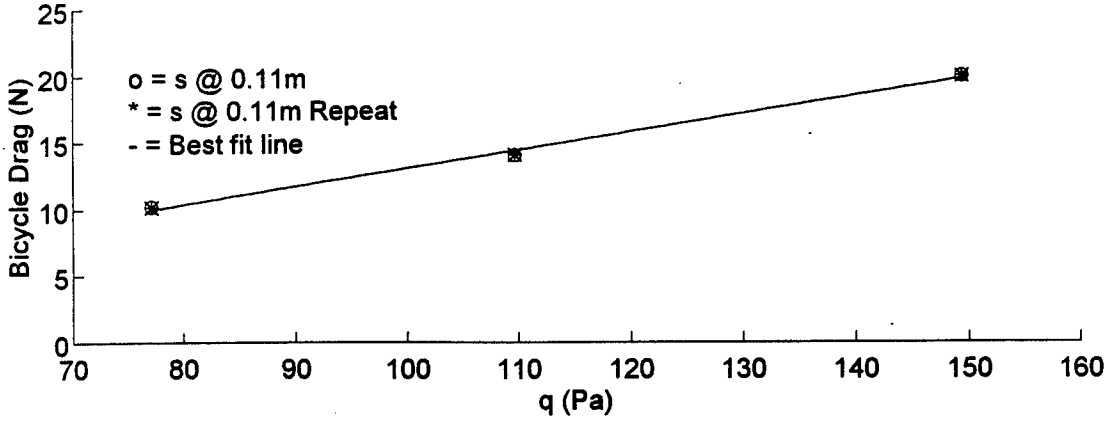

Figure 19. Repeatabilty Check, Bicycle Model

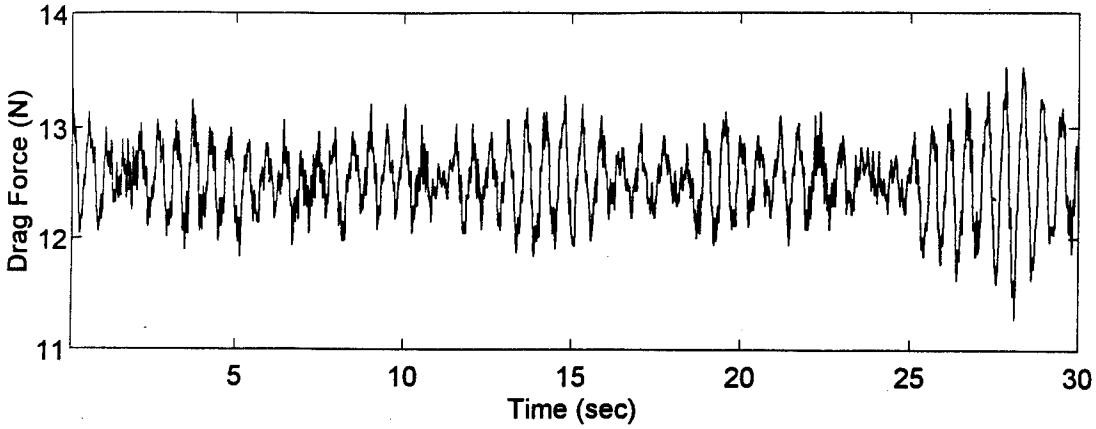

Figure 20. Variation of Drag with Time, Bicycle Model

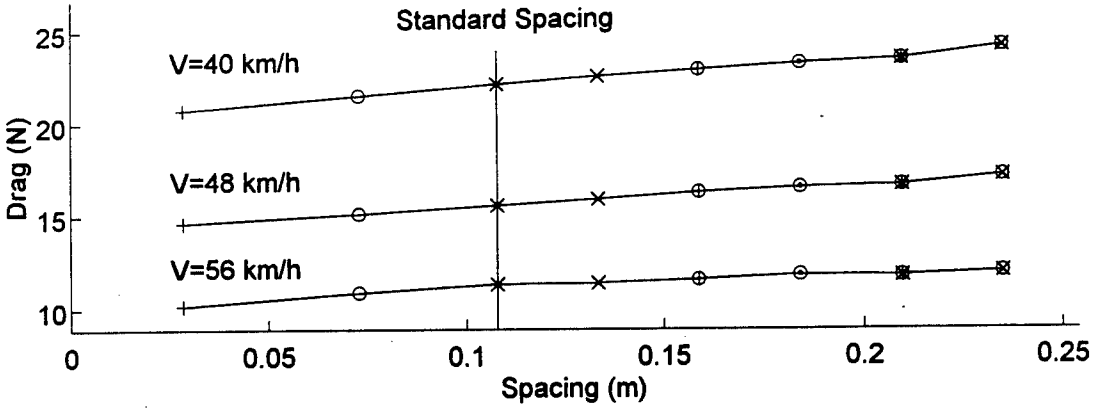

Figure 21. Effect of Spacing on Total Drag, Open Frame, Rotating Wheel

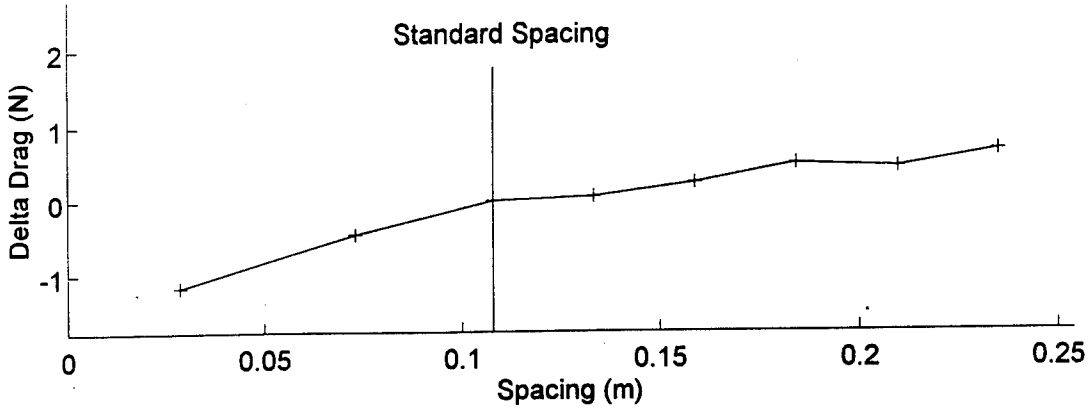

Figure 22. Effect of Spacing on Change in Drag, 40 km/h

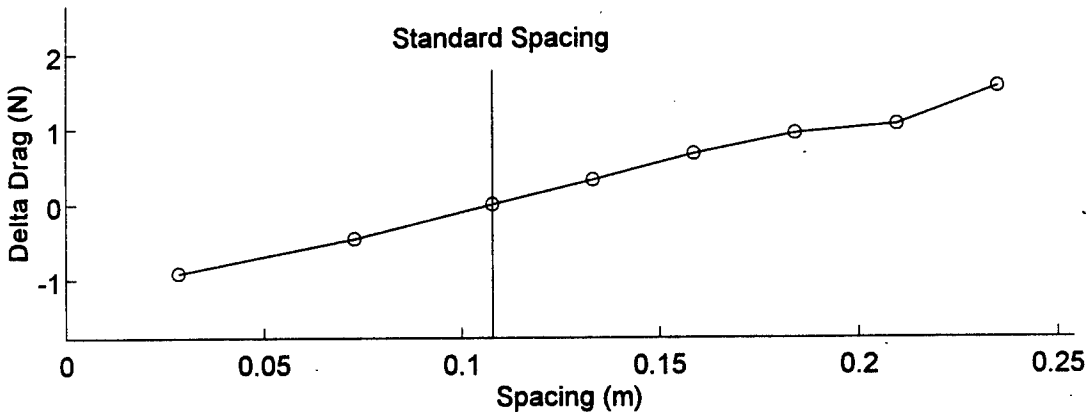

Figure 23. Effect of Spacing on Change in Drag, 48 km/h

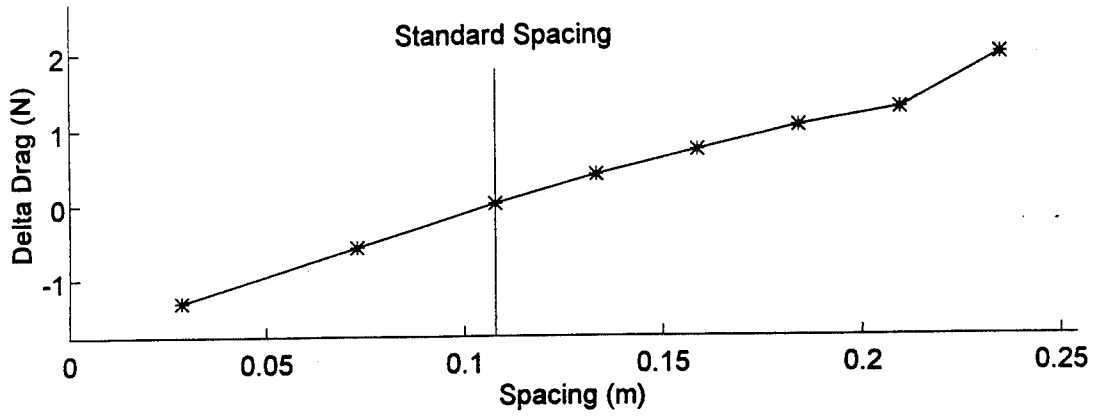

Figure 24. Effect of Spacing on Change in Drag, 56 km/h

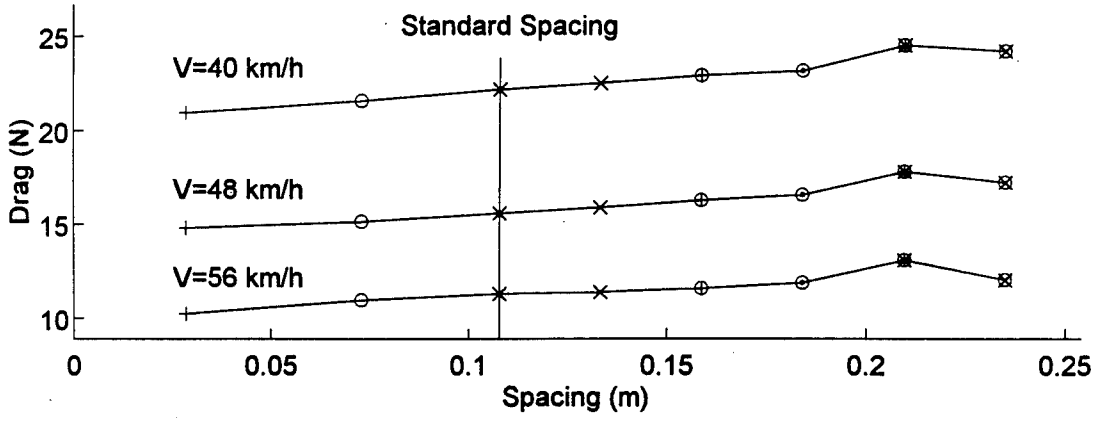

Figure 25. Effect of Spacing on Total Drag, Open Frame, Static Wheel

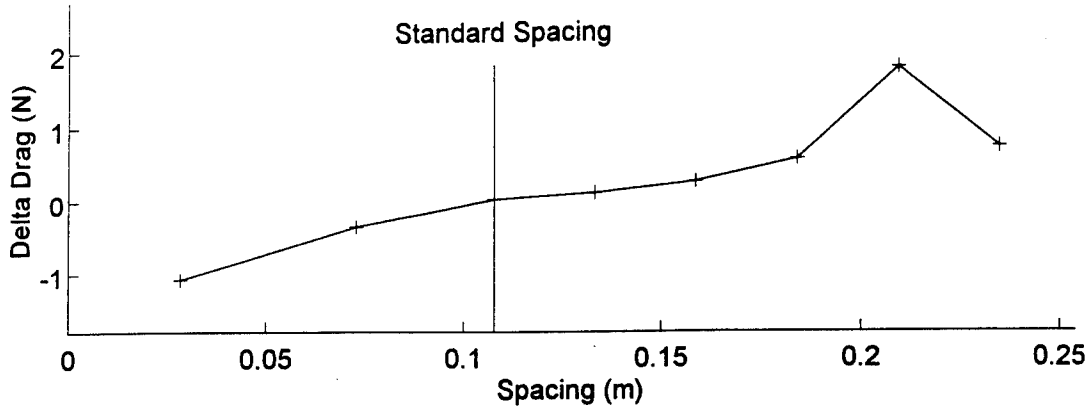

Figure 26. Effect of Spacing on Change in Drag, 40 km/h

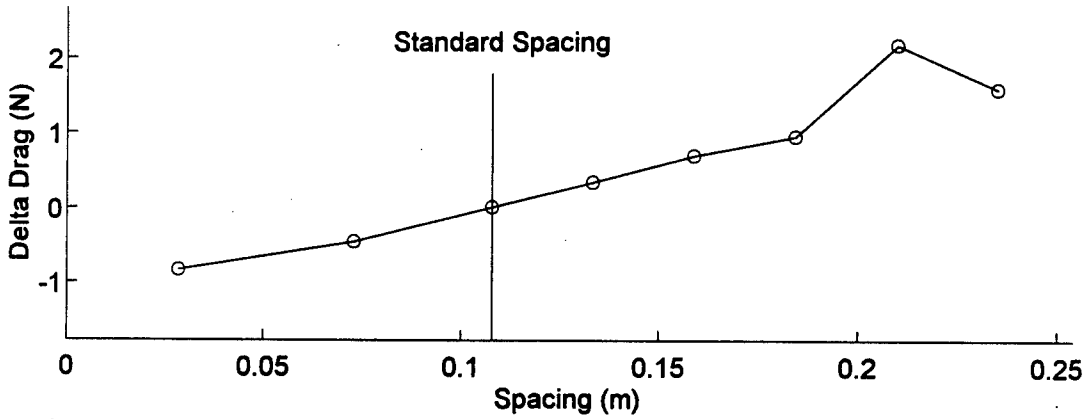

Figure 27. Effect of Spacing on Change in Drag, 48 km/h

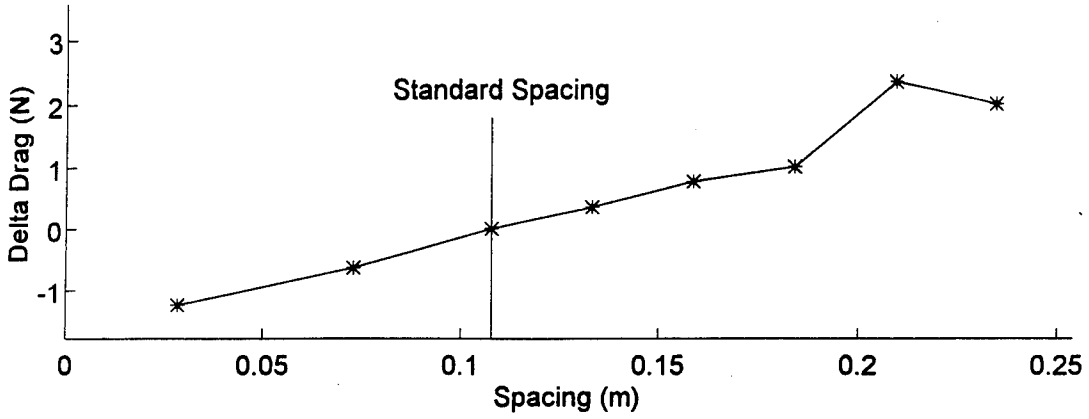

Figure 28. Effect of Spacing on Change in Drag, 56 km/h

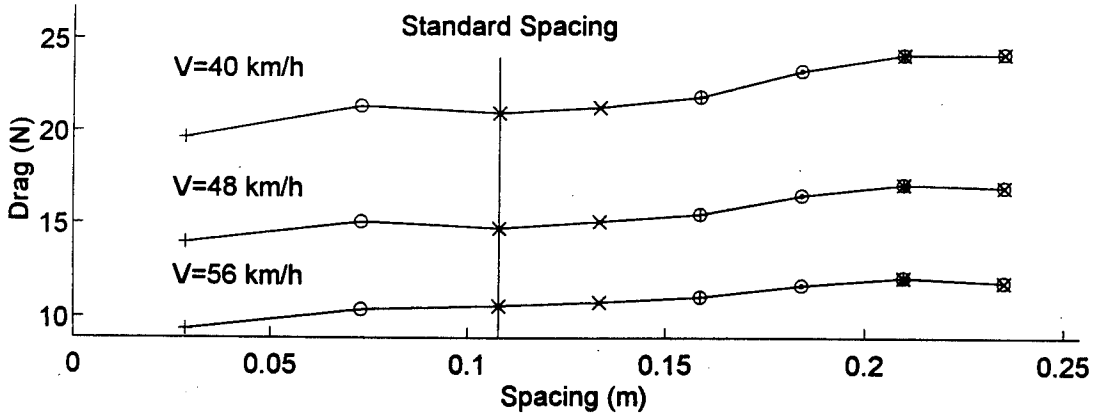

Figure 29. Effect of Spacing on Total Drag, Closed Frame, Rotating Wheel

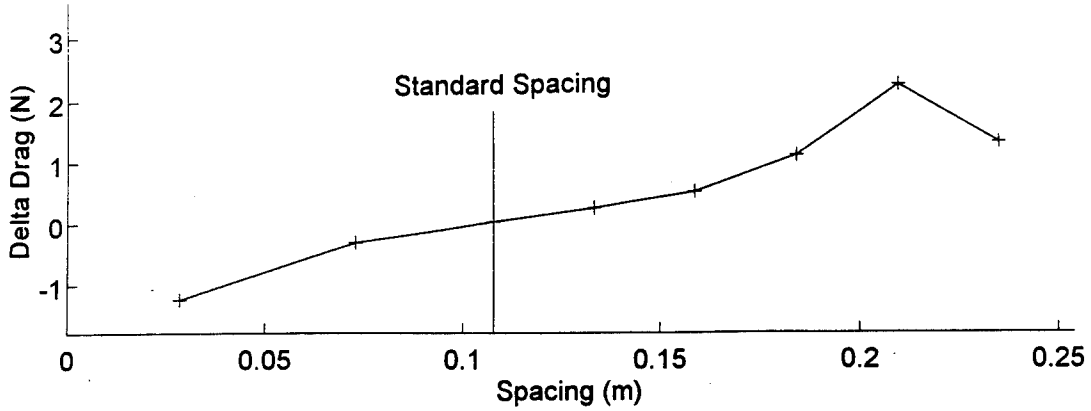

Figure 30. Effect of Spacing on Change in Drag, 40 km/h

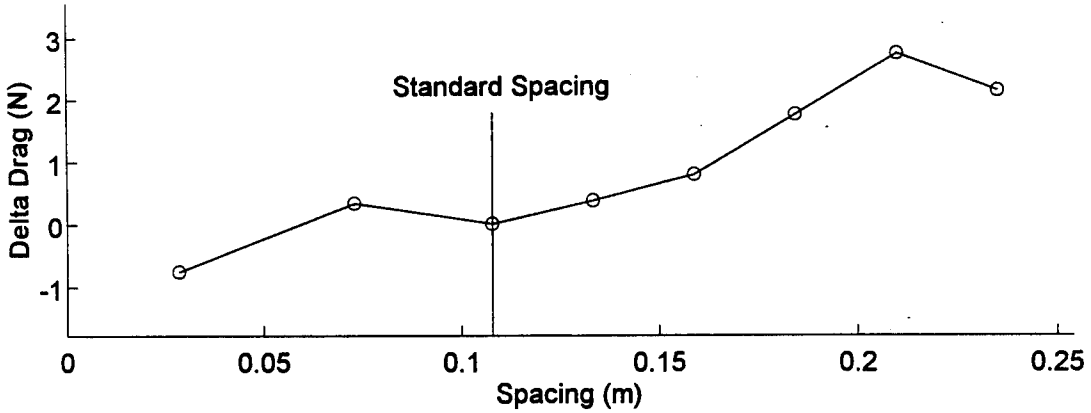

Figure 31. Effect of Spacing on Change in Drag, 48 km/h

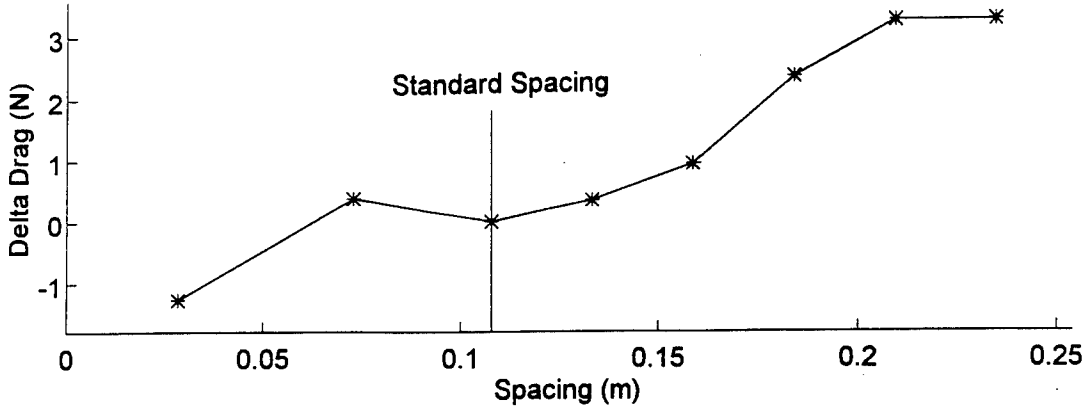

Figure 32. Effect of Spacing on Change in Drag, 56 km/h

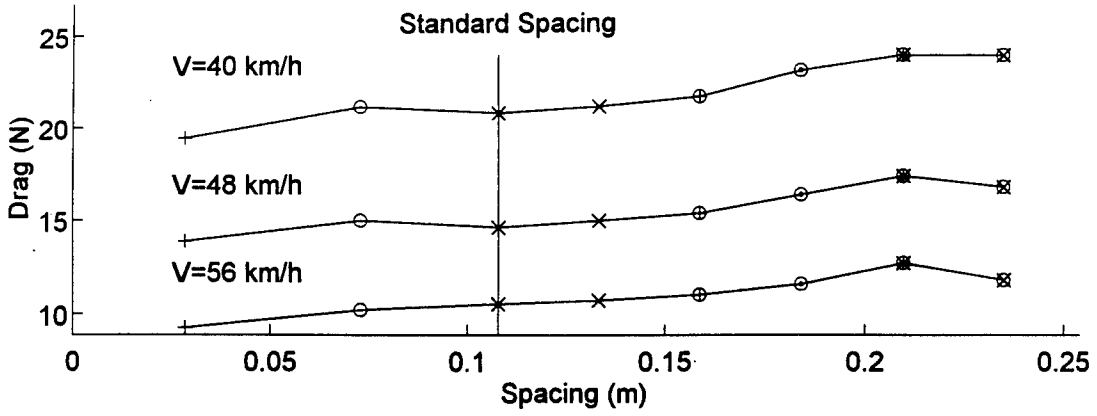

Figure 33. Effect of Spacing on Total Drag,Closed Frame, Static Wheel

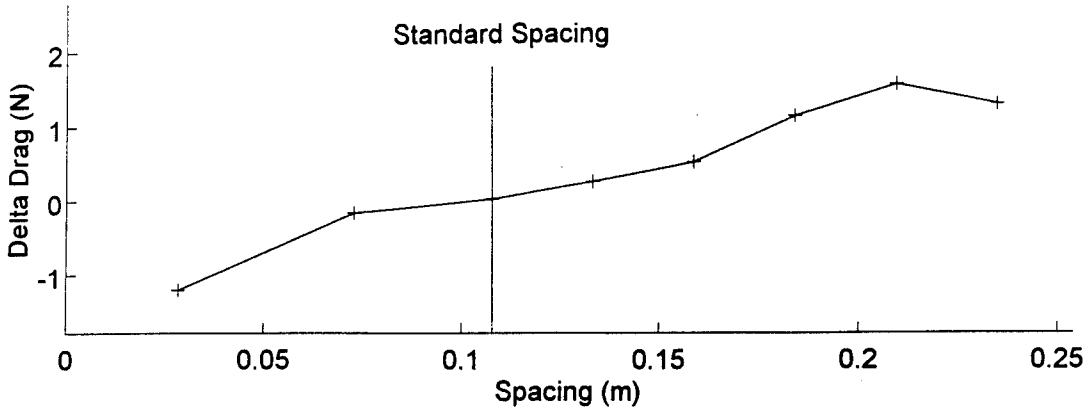

Figure 34. Effect of Spacing on Change in Drag, 40 km/h

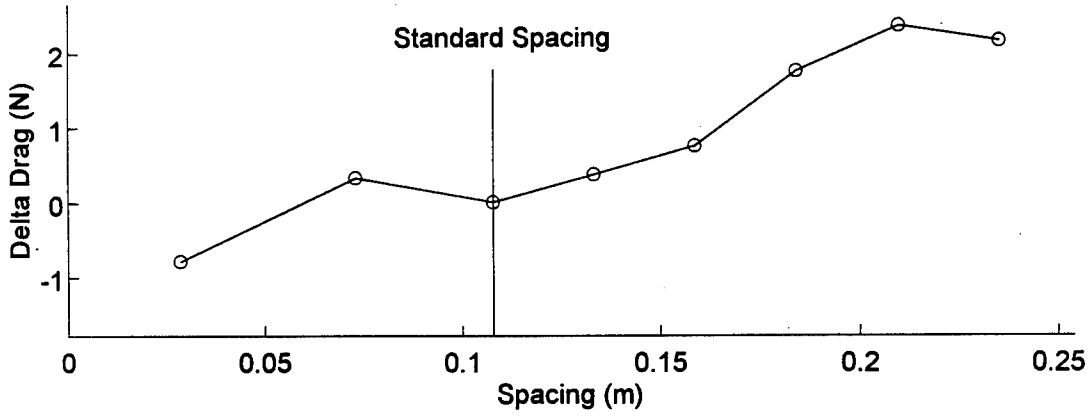

Figure 35. Effect of Spacing on Change in Drag, 48 km/h

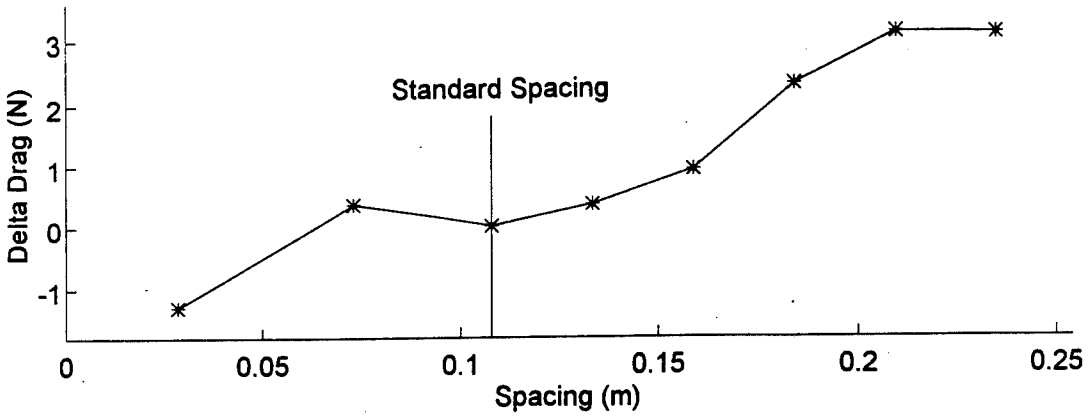

Figure 36. Effect of Spacing on Change in Drag, 56 km/h

APPENDIX A. ERROR ANALYSIS

There are many ways to determine and overall estimate of error for a given calculation that is based on several measurements. For this study the error was estimated using the standard error method. This method provides a root sum square most probable error estimate. The error is determined from

$$Error_{RSS} = \sqrt{(\Delta u_1 \frac{\partial s}{\partial u_1})^2 + (\Delta u_2 \frac{\partial s}{\partial u_2})^2 + \ldots}$$

where Δu_1 is the uncertainty of that particular parameter in the calculation and $\frac{\partial s}{\partial u}$ is the sensitivity of the calculation to that parameter.

The axial force, or drag, was calculated from the reduction formula

$$Drag = \frac{1}{m}(\frac{V_{out}}{E_{in}} - \frac{V_{zero}}{E_{zero}} - b)$$

where m and b are the slope and intercept from the flexure calibration curve, V_{in} and E_{zero} are the loaded and zero point output voltages, respectively, but normalized by E_{in} and E_{zero}, the bridge excitation voltages for those conditions. The standard error then for the force calculation is

$$Error_{Force} = \sqrt{\left(\frac{\Delta V_{in}}{mE_{in}}\right)^2 + \left(\frac{-V_{in}\Delta E_{in}}{mE_{in}^{\ 2}}\right)^2 + \left(\frac{-\Delta V_{zero}}{mE_{zero}}\right)^2 + \left(\frac{V_{zero}\Delta E_{zero}}{mE_{zero}^{\ 2}}\right)^2}$$

where the uncertainty quantities are according to Table 6.

Table 6. Component Uncertainties

Component	Uncertainty (Volts)
ΔV_{in}	48.8e-6
ΔE_{in}	4.8e-3
ΔV_{zero}	48.8e-6
ΔE_{zero}	4.8e-3

Note that, the sensitivity and error due to the calibration slope and intercept are zero since the calibration resulted in correlation coefficients of 0.99999.

Application of the above to the collected data resulted in the following estimated errors. For the cylinder data collected with the single component balance, the typical error for a data set was estimated at 0.053 N (0.012 lb_f). Similarly, the bicycle data for the single component balance yielded typical errors of 0.049 N (0.011 lb_f). These values compare to static check load results that showed errors of 0.022 N (0.005 lb_f). The standard error is thus conservative but also accounts for the uncertainty associated with a dynamic measurement. For the cylinder data collected with the commercial balance, the error was estimated based on the information provided by the manufacturer. In this case, the error is 1% of the full scale load of 222.41 N (50 lb_f) or 2.22 N (0.5 lb_f).

APPENDIX B. ENGLISH UNIT FIGURES

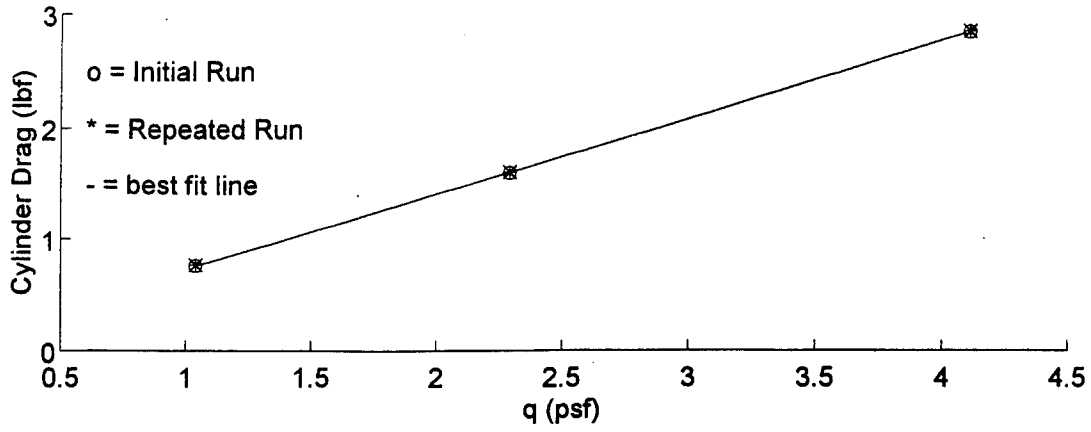

Figure 12. Repeatability Check, Six Component Balance

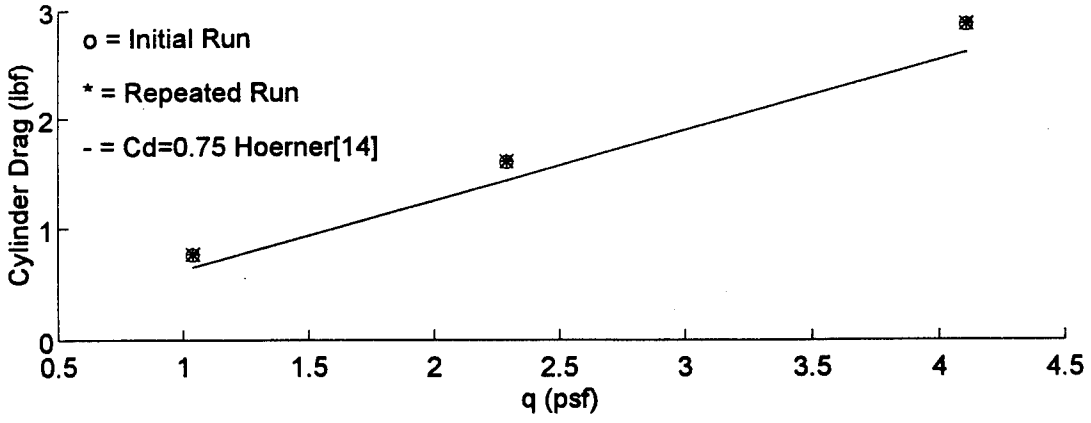

Figure 13. Comparison of Drag with Previous Results, Six Component Balance

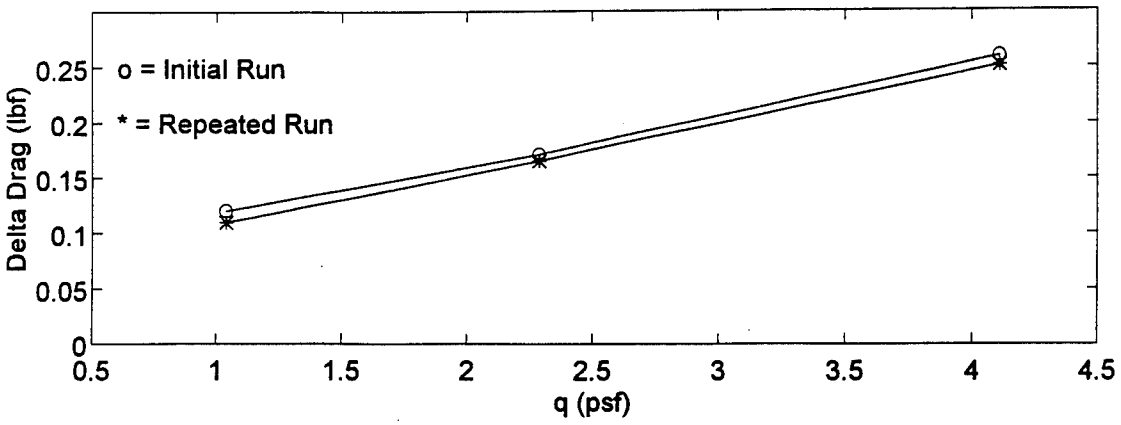

Figure 14. Difference in Drag with Previous Results, Six Component Balance

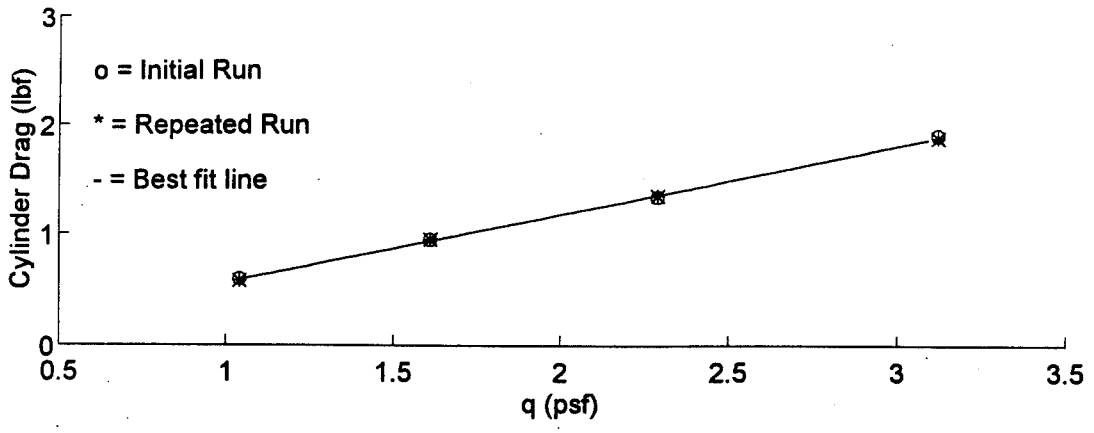

Figure 15. Repeatabilty Check, Single Component Balance

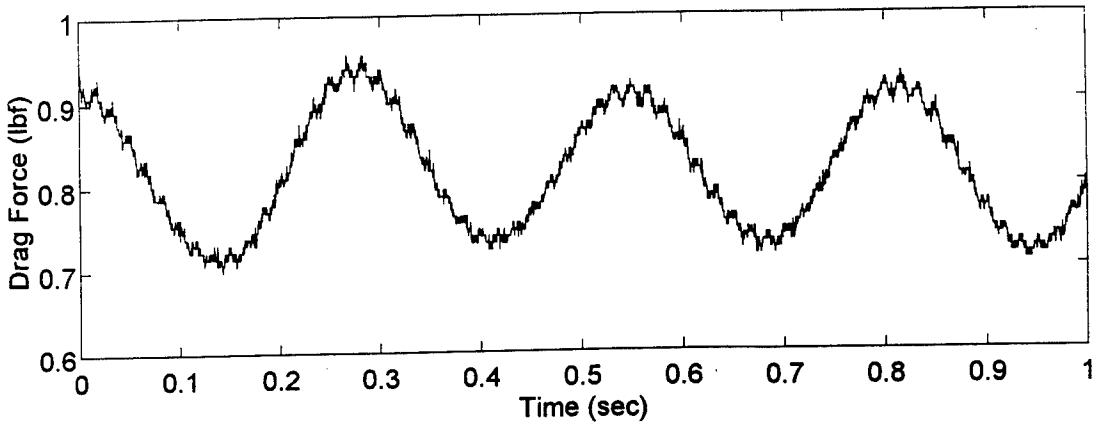

Figure 16. Variation of Drag with Time, Single Component Balance

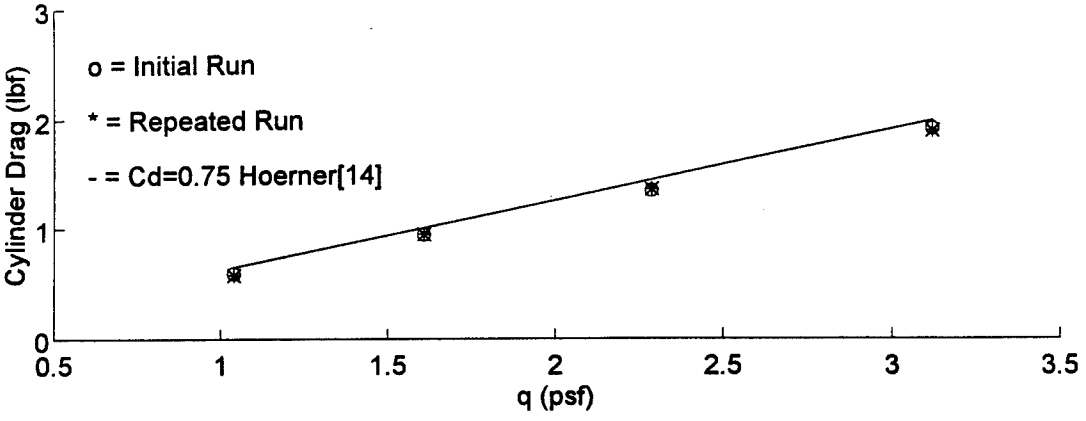

Figure 17. Comparison of Drag with Previous Results, Single Component Balance

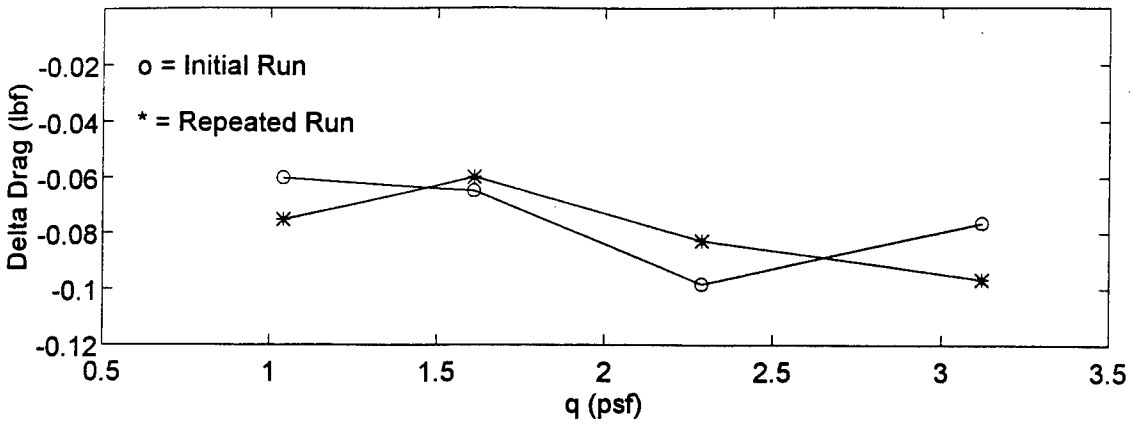

Figure 18. Difference in Drag with Previous Results, Single Component Balance

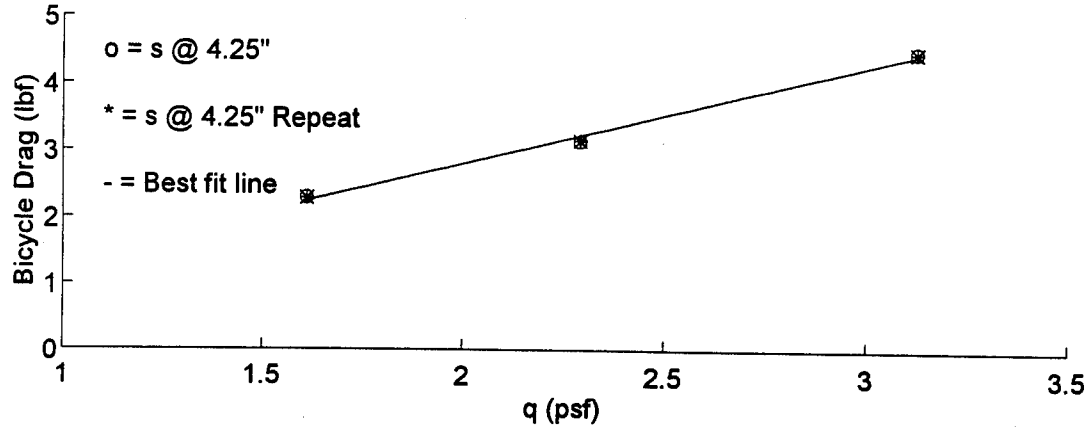

Figure 19. Repeatabilty Check, Bicycle Model

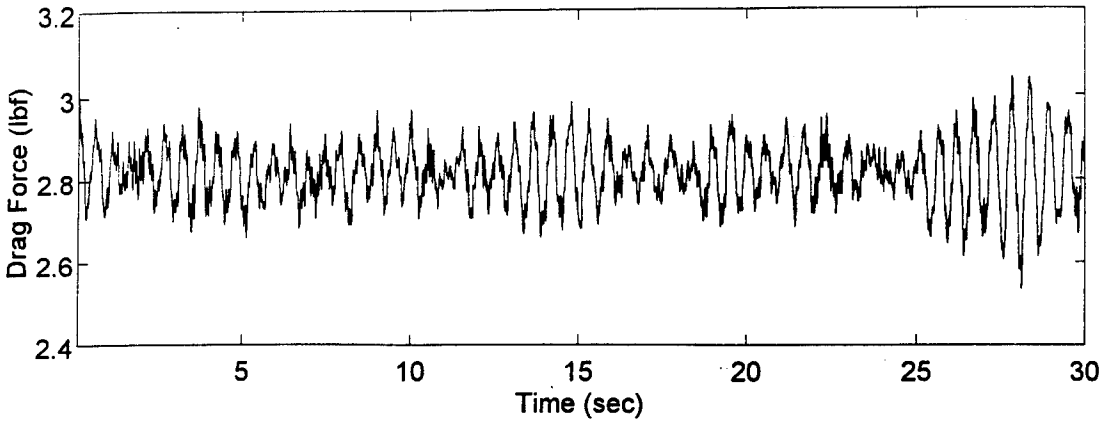

Figure 20. Variation of Drag with Time, Bicycle Model

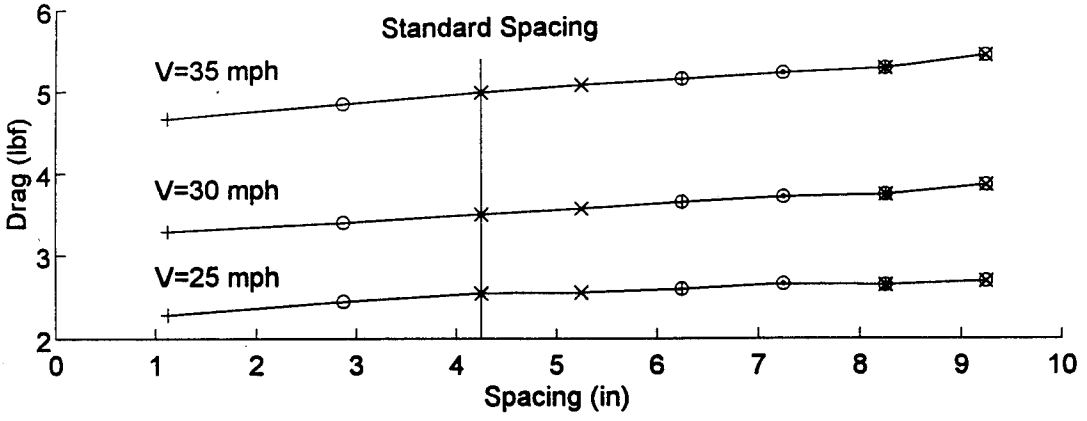

Figure 21. Effect of Spacing on Total Drag, Open Frame, Rotating Wheel

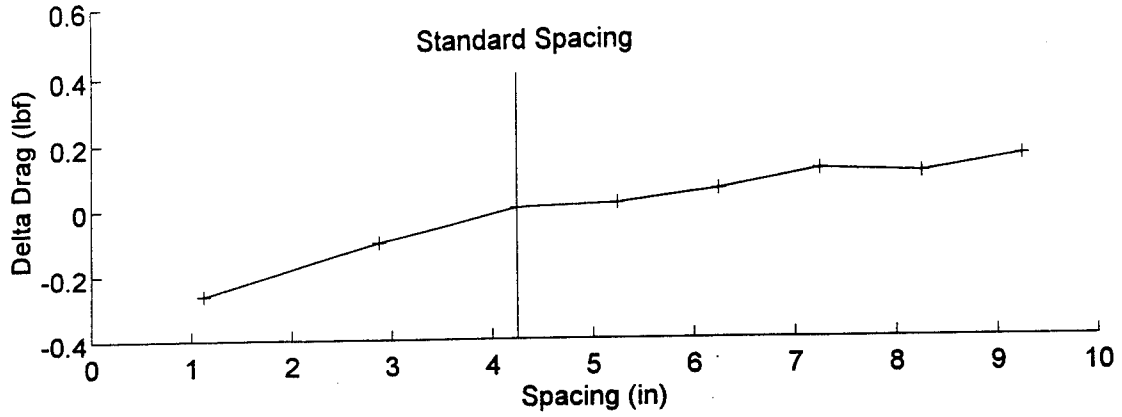

Figure 22. Effect of Spacing on Change in Drag, 25 mph

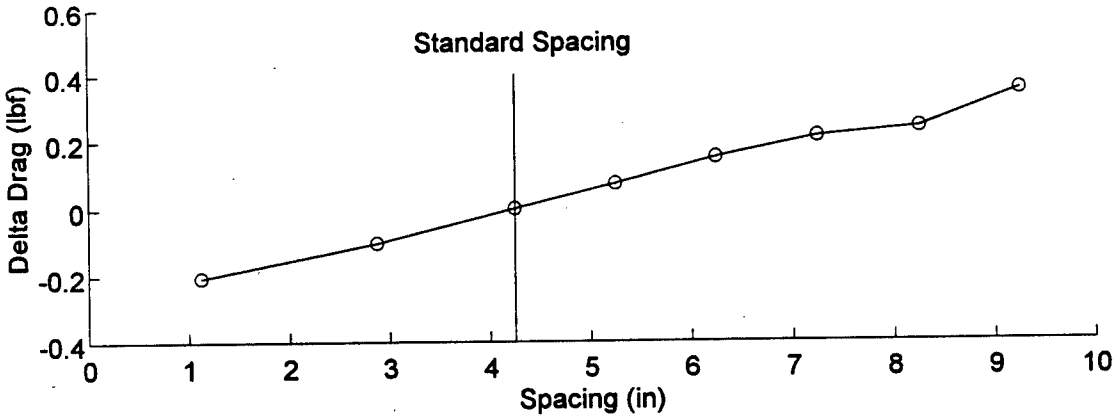

Figure 23. Effect of Spacing on Change in Drag, 30 mph

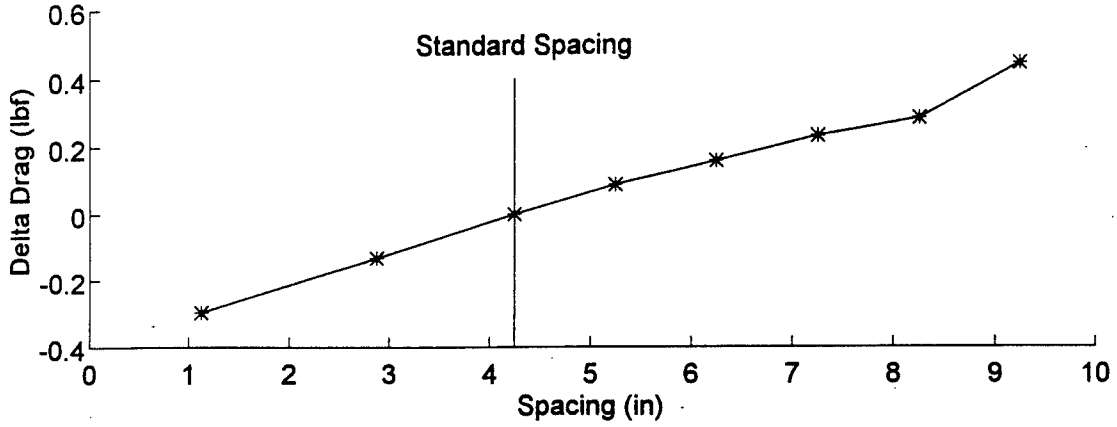

Figure 24. Effect of Spacing on Change in Drag, 35 mph

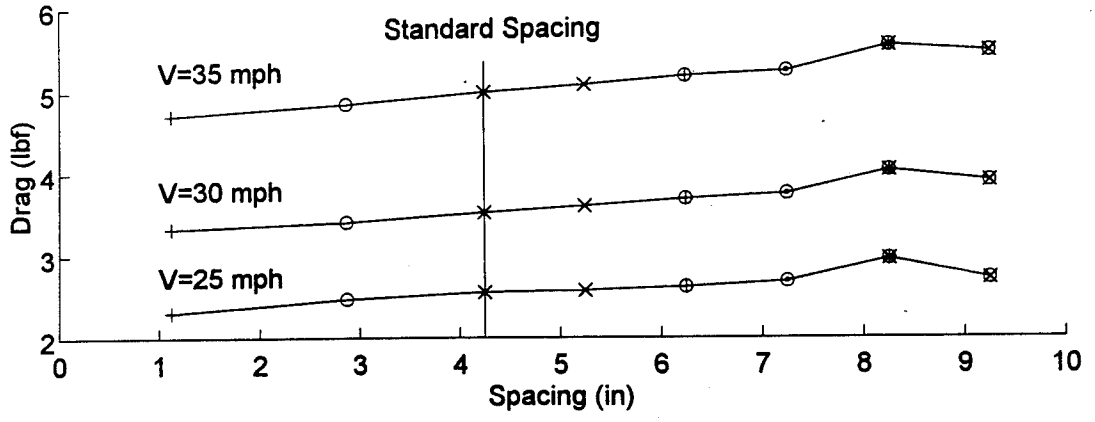

Figure 25. Effect of Spacing on Total Drag, Open Frame, Static Wheel

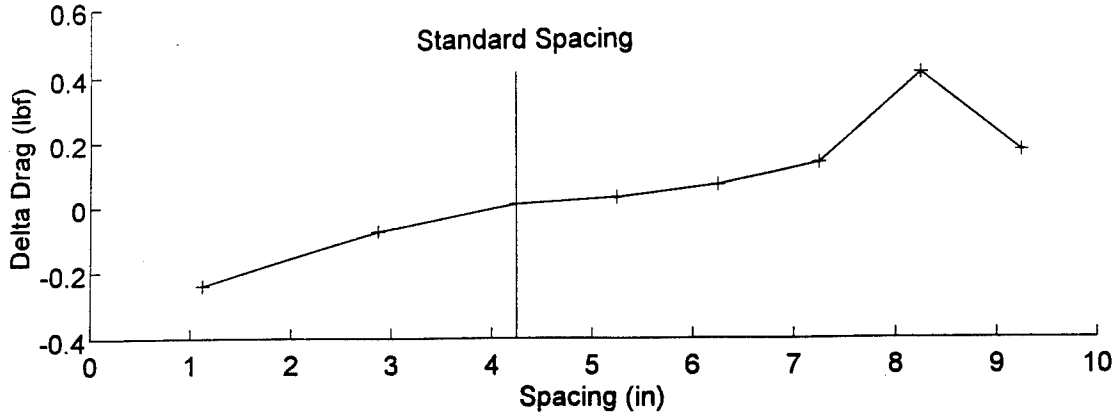

Figure 26. Effect of Spacing on Change in Drag, 25 mph

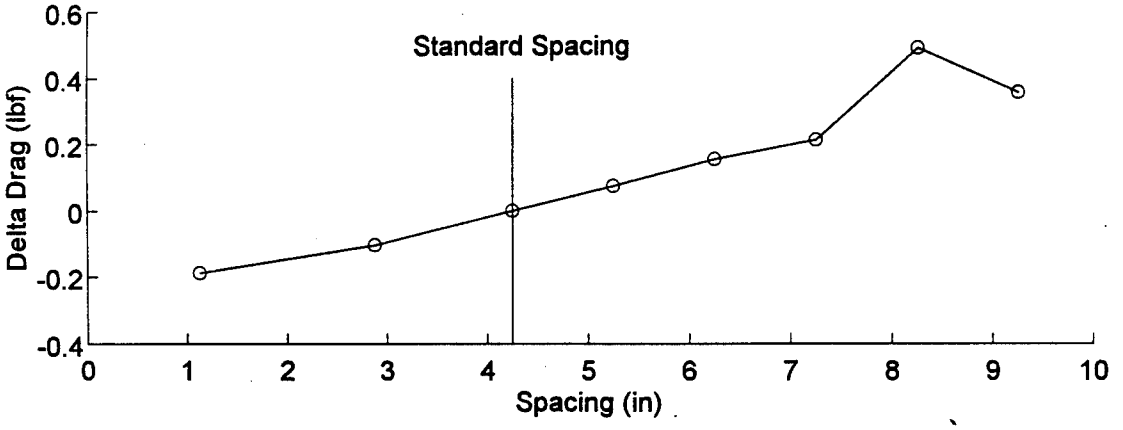

Figure 27. Effect of Spacing on Change in Drag, 30 mph

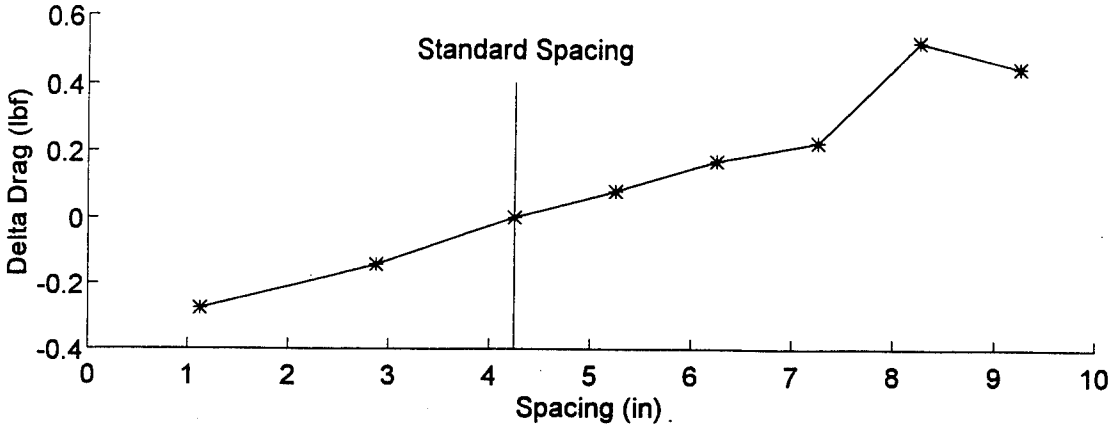

Figure 28. Effect of Spacing on Change in Drag, 35 mph

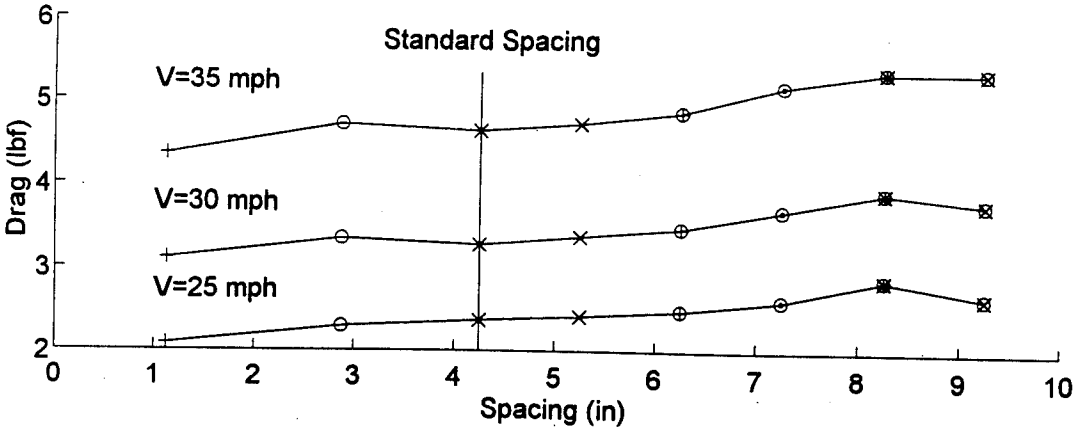

Figure 29. Effect of Spacing on Total Drag, Closed Frame, Rotating Wheel

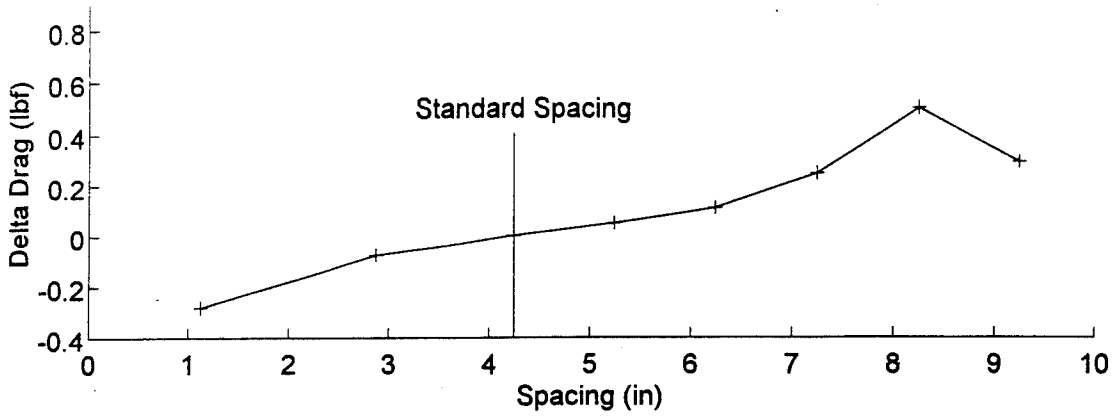

Figure 30. Effect of Spacing on Change in Drag, 25 mph

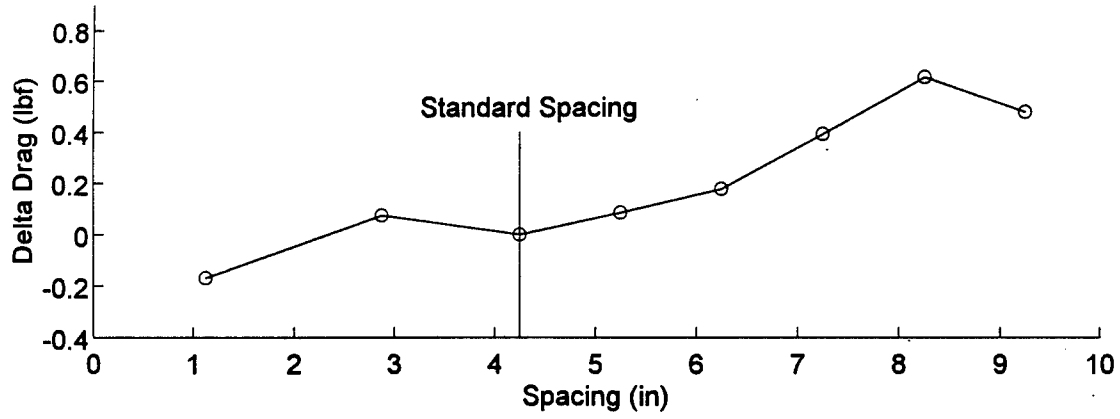

Figure 31. Effect of Spacing on Change in Drag, 30 mph

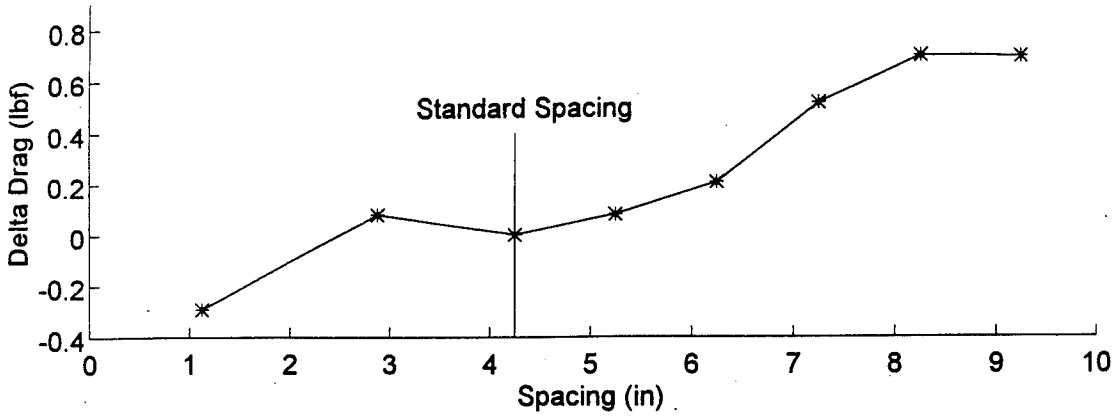

Figure 32. Effect of Spacing on Change in Drag, 35 mph

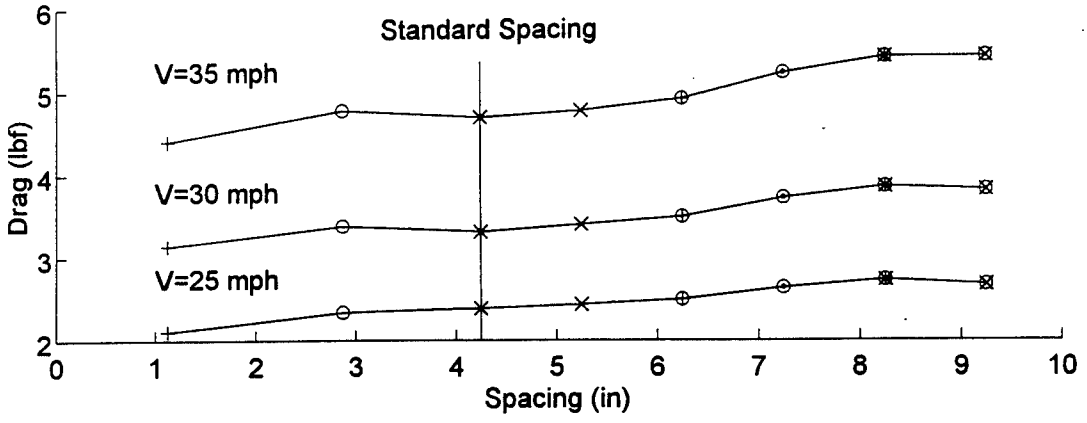

Figure 33. Effect of Spacing on Total Drag,Closed Frame, Static Wheel

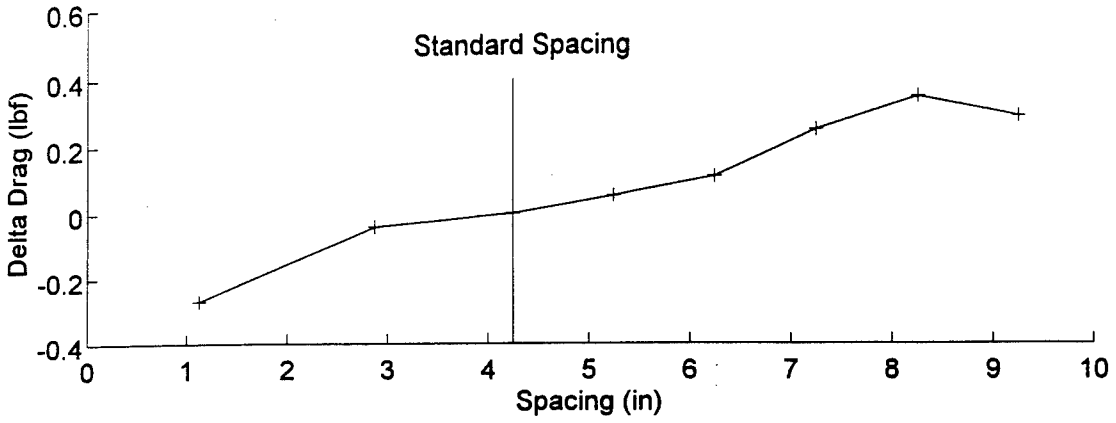

Figure 34. Effect of Spacing on Change in Drag, 25 mph

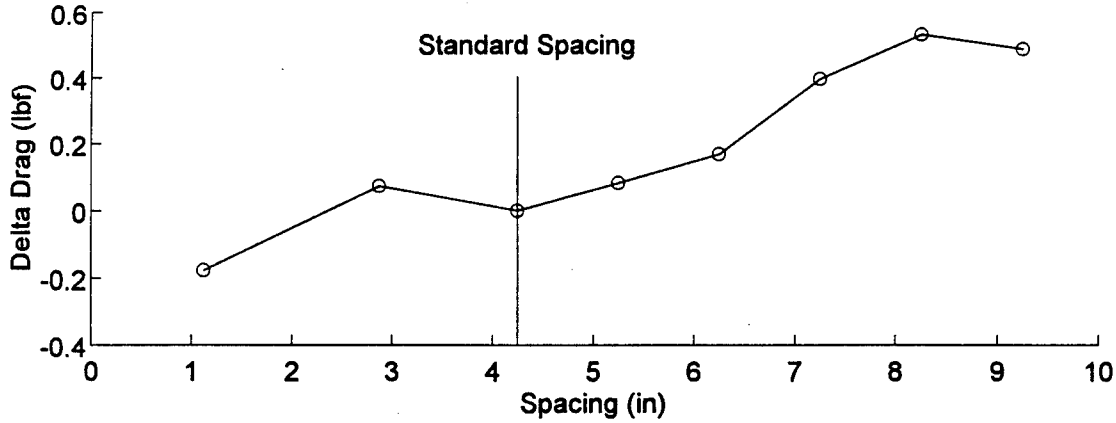

Figure 35. Effect of Spacing on Change in Drag, 30 mph

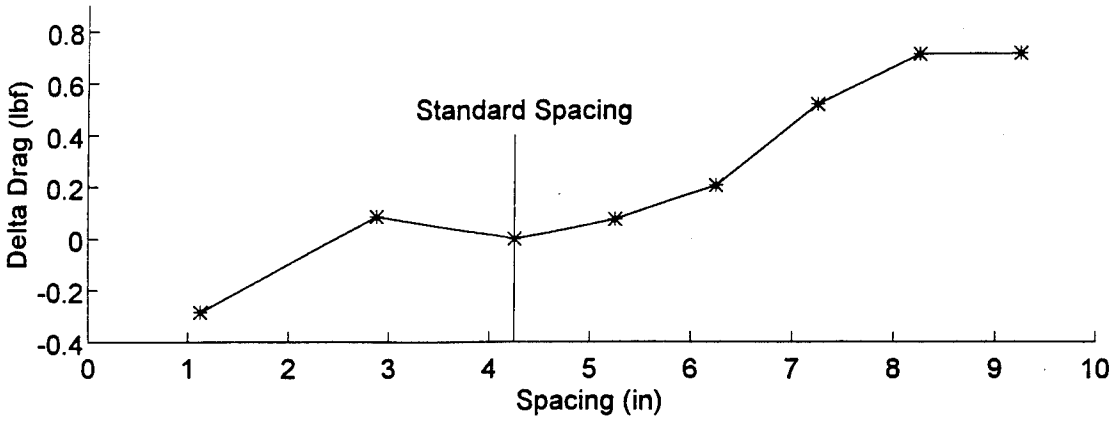

Figure 36. Effect of Spacing on Change in Drag, 35 mph

VITA

Captain Brian A. Parker was born in Phoenix, Arizona on February 10, 1966. He graduated from Moon Valley High School in Phoenix in 1984 and subsequently attended the University of Southern California in Los Angeles, California. After graduating with a bachelor's degree in Aerospace Engineering and earning a regular commission from Reserve Officer Training Corp (ROTC), his first assignment was to Los Angeles AFB, El Segundo, CA. He served in the Titan IV and Global Positioning System (GPS) Program Offices.

Permanent Address: 3671 Winston Churchill Drive
Beavercreek, Ohio 45432

REPORT DOCUMENTATION PAGE

Form Approved
OMB No. 0704-0188

1. AGENCY USE ONLY (Leave blank)	2. REPORT DATE	3. REPORT TYPE AND DATES COVERED
	December 1994	Master's Thesis

4. TITLE AND SUBTITLE
A New Drag Measurement System for Wind Tunnel Testing of the Racing Bicycle and Rider to Determine a Low Drag Configuration

5. FUNDING NUMBERS

6. AUTHOR(S)
Brian A. Parker

7. PERFORMING ORGANIZATION NAME(S) AND ADDRESS(ES)
Air Force Institute of Technology, WPAFB, OH 45433-6583

8. PERFORMING ORGANIZATION REPORT NUMBER
AFIT/GAE/ENY/94D-17

9. SPONSORING / MONITORING AGENCY NAME(S) AND ADDRESS(ES)
Bruce Campbell
WL/XPT Bldg 45
2130 Eighth St. Ste 1
Wright-Patterson AFB OH 45433-6523

10. SPONSORING / MONITORING AGENCY REPORT NUMBER

11. SUPPLEMENTARY NOTES

12a. DISTRIBUTION / AVAILABILITY STATEMENT
Approved for public release; distribution unlimited

12b. DISTRIBUTION CODE

13. ABSTRACT *(Maximum 200 words)*

This study investigated the application of splitter plate effects to reduce the aerodynamic drag of the racing bicycle and rider system. A sensitive, low-force, beam-type, single-component balance was developed to provide drag measurements accurate to within 0.053 N (0.012 lb_f). The performance of the new system was verified by comparing the measured drag on a three-dimensional, right-circular cylinder model, 0.127 m (5.0 in) in diameter and 0.610 m (24 in) long, with the results from a commercial balance and a other similar data. The bicycle and rider model consisted of a full-scale mannequin comprising only the hips, legs and feet, mounted on a regulation 0.48 m (19 in) size bicycle. Rotation of the wheels and a stationary ground plane were also simulated. Two frame configurations in conjunction with a disk type wheel were tested to determined the lowest drag configuration for narrow and wide spacing of the rider's legs. The results show that for the standard tube construction frame, the conventional wisdom to streamline as much as possible prevails. When an aerodynamic frame was tested, the overall drag was reduced. Although the standard spacing still provided the lowest drag configuration, any further streamlining showed an increase in drag.

14. SUBJECT TERMS	15. NUMBER OF PAGES
wind tunnel tests, aerodynamic drag, drag reductions, vehicles	91
	16. PRICE CODE

17. SECURITY CLASSIFICATION OF REPORT	18. SECURITY CLASSIFICATION OF THIS PAGE	19. SECURITY CLASSIFICATION OF ABSTRACT	20. LIMITATION OF ABSTRACT
Unclassified	Unclassified	Unclassified	UL